


Learning under Distributional Drift: Reproducibility as an Intrinsic Statistical Resource

Sofiya C Zaichyk 

Innovative Defense Technologies

Abstract

Statistical learning under distributional drift remains insufficiently characterized: when each observation alters the data-generating law, classical generalization bounds can collapse. We introduce a new statistical primitive, the *reproducibility budget* C_T , which quantifies a system’s finite capacity for *statistical reproducibility*—the extent to which its sampling process can remain governed by a consistent underlying distribution in the presence of both exogenous change and endogenous feedback. Formally, C_T is defined as the cumulative Fisher–Rao path length of the coupled learner–environment evolution, measuring the total distributional motion accumulated during learning. From this construct we derive a drift–feedback generalization bound of order $O(T^{-1/2} + C_T/T)$, and we prove a matching minimax lower bound showing that this rate is minimax-optimal. Consequently, the results establish a *reproducibility speed limit*: no algorithm can achieve smaller worst-case generalization error than that imposed by the average Fisher–Rao drift rate C_T/T of the data-generating process. The framework situates exogenous drift, adaptive data analysis, and performative prediction within a common geometric structure, with C_T emerging as the intrinsic quantity measuring distributional motion across these settings.

Keywords: information geometry, statistical learning theory, non-stationary learning, generalization bounds, distributional shift

1 Introduction

Modern learning systems often operate in *self-modifying environments*, where learning alters the very distribution it learns from. A recommender policy reshapes user preferences as it updates (Perdomo et al., 2020); adaptive experiments change the distribution from which subsequent data are drawn (Li et al., 2024); and reinforcement-driven agents modify the state transitions that determine future feedback (Sutton and Barto, 2018; Even-Dar and Mansour, 2003; Åström and Murray, 2008). In all such cases, the learner is not a passive observer of a stationary process but an active participant in an evolving distributional flow. This feedback coupling breaks not only stationarity but the assumption of *statistical reproducibility*—that future data could, in principle, be redrawn from the same law (Vapnik, 1998).

1.1 Motivation

Given samples $\{(x_i, y_i)\}_{i=1}^T$ drawn i.i.d. from a fixed distribution $p(x, y)$, population and empirical risks coincide asymptotically, with convergence rate $O(T^{-1/2})$ (Vapnik, 1998). Once the data-generating process itself changes, these guarantees collapse. When distributional shift depends on the learner’s trajectory, the change is no longer exogenous but *endogenous*: a function of the learner’s own actions and their cumulative impact on the environment. In such settings, convergence is governed not by sample size, but by how far the underlying distribution moves over the course of learning, a quantity naturally measured in the statistical geometry of the model.

Consider an adaptive recommender with policy π_t that selects content for users while updating its model from observed responses. Each recommendation depends on past data yet also shapes

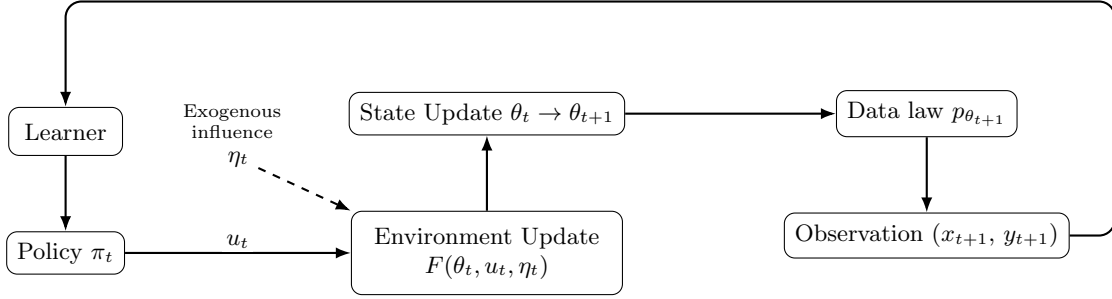


Figure 1. Coupled drift process. The learner’s policy π_t and exogenous influence η_t act on the environment, evolving θ_t to θ_{t+1} under $F(\theta_t, u_t, \eta_t)$. This new state defines the next data distribution $p_{\theta_{t+1}}$, closing the feedback loop. Exogenous factors η_t perturb θ_t externally, while endogenous feedback arises from the learner’s own actions.

future data, since user preferences evolve with exposure. Let the environment be parameterized by θ_t , governing $p_{\theta_t}(x, y)$, and evolve according to

$$(x_t, y_t) \sim p_{\theta_t}, \quad \theta_{t+1} = F(\theta_t, u_t), \quad u_t \sim \pi_t(\mathcal{F}_t), \quad (1)$$

where \mathcal{F}_t is the filtration of all past observations and u_t is some action chosen by the learner. Even if F is smooth and deterministic, its dependence on u_t ensures that θ_{t+1} reflects the learner’s internal decisions, producing a coupled stochastic process with a natural Fisher–Rao geometry. The family $\{p_\theta\}$ forms a statistical manifold whose intrinsic Riemannian metric—the Fisher information—measures how sensitively the distribution changes under infinitesimal perturbations of θ . Thus the learner–environment interaction induces geometric motion in Fisher–Rao distance. The resulting sequence $\{(x_t, y_t)\}$ is *non-reproducible*: rerunning the same algorithm would yield a distinct trajectory unless the entire feedback loop were exactly replicated.

The same feedback-driven non-reproducibility arises in adaptive testing, model-in-the-loop simulation, and autonomous control. This raises a fundamental question: how far can the learner–environment system move before classical guarantees break? To answer this, we develop a geometric framework for quantifying distributional motion during learning. Across these closed-loop regimes, we analyze this coupling at the level of statistical generalization, showing that diverse non-stationary settings emerge as special cases of a single geometric bound governed by a finite reproducibility budget.

1.2 Conceptual View

We view the data-generating process as a trajectory $\{\theta_t\}$ on a statistical manifold, whose discrete path length represents cumulative information change (Amari and Nagaoka, 2000). Any smooth divergence admits a second-order expansion whose Hessian defines a local Riemannian metric (Amari, 2016). For the broad class of f -divergences, including KL, χ^2 , Hellinger, and α -divergences, this induced metric coincides with the Fisher–Rao geometry. Fisher–Rao is therefore the canonical *invariant* Riemannian metric on a statistical model (Čencov, 1982; Amari and Nagaoka, 2000). It is preserved under smooth reparameterizations and captures displacement intrinsic to the model family rather than to any particular coordinate system. Although different divergences quantify global discrepancies between distributions, their local quadratic structure collapses to the same information metric, and only the Fisher metric enjoys this invariance property (Čencov, 1982). At an infinitesimal scale, Fisher information provides the quadratic form that linearizes KL divergence and characterizes the distinguishability of nearby models. This is not a peculiarity of KL, but a reflection of the shared second-order geometry of all f -divergences. Consequently, Fisher–Rao arc

length offers a natural intrinsic scale for describing how small distributional perturbations alter the statistical environment of a learner.

Accumulating these infinitesimal displacements yields an intrinsic Riemannian arc length (Amari and Nagaoka, 2000). This differs fundamentally from summing TV, Wasserstein, or KL increments, which are extrinsic divergences and do not compose additively along a path. What the arc length measures is not merely “how far the distribution moved” in a chosen divergence, but the total statistical distinguishability expended along the trajectory in the unique geometry that governs estimation. Generalization error then depends not only on the number of samples but also on the total path length traversed by the data distribution during learning.

Definition 1 (Statistical Reproducibility) *Reproducibility is a statistical property of a learning process: the extent to which repeated executions of the same algorithm would sample from comparable data-generating laws. Let $p_{\theta_t}(x, y)$ denote the distribution at time t and g_θ the Fisher–Rao metric on Θ . The reproducibility budget*

$$C_T = \sum_{t=1}^T \|\Delta\theta_t\|_{g_{\theta_t}}$$

quantifies the cumulative Fisher–Rao path length of the trajectory $\{\theta_t\}$ and hence the total loss of reproducibility incurred during learning. The term “budget” emphasizes that reproducibility is finite. Each Fisher–Rao displacement consumes part of the available geometric capacity for drawing comparable samples. When C_T grows large, reproducibility is exhausted.

Although the quantity C_T is defined as the Fisher–Rao path length of the trajectory, its role in generalization is not assumed. Rather, the dependence of the risk on C_T follows from the Fisher–Rao geometry and is shown to be minimax-optimal in Theorem 15.

While C_T measures total Fisher–Rao distance, the motion of θ_t may arise from distinct causes. Some displacement is *exogenous*, driven by external change. The rest is *endogenous*, reflecting how the learner’s own policy alters the data-generating law. Decomposing each step’s Fisher length into these components gives

$$C_T = \sum_{t=1}^T (d_t + \alpha \kappa_t^{(\mathcal{M})}), \quad (2)$$

where d_t captures environment-driven motion, $\kappa_t^{(\mathcal{M})}$ captures policy-sensitive motion, and α balances their contribution. The budget C_T is intrinsic—the Fisher–Rao path length of the trajectory. The decomposition into d_t and $\kappa_t^{(\mathcal{M})}$ is carried out entirely within the same Riemannian geometry, where both terms are derived from the Fisher metric and together approximate $\|\Delta\theta_t\|_{g_{\theta_t}}$. What is model-dependent is only which directions of the tangent space are activated by the environment versus the learner, not the geometric structure of the decomposition itself.

Our results show that the expected generalization deviation satisfies

$$\mathbb{E} |\hat{R}_T - R_T| \leq C_0 T^{-1/2} + C_1 T^{-1} \sum_t d_t + C_2 T^{-1} \sum_t \kappa_t^{(\mathcal{M})}, \quad (3)$$

and that no algorithm operating within this drift–feedback model can improve upon the asymptotic rate $\Theta(T^{-1/2} + C_T/T)$. This defines a *reproducibility speed limit*: no learner can achieve smaller worst-case generalization error than that imposed by the average Fisher–Rao drift rate C_T/T of the data-generating process. Earlier analyses bounded distributional change through variation or information budgets. Those quantities are extrinsic and problem-specific. The reproducibility budget C_T is intrinsic. It is defined directly on the statistical manifold and admits a matching lower bound that prior formulations lack. It provides a geometric quantity that can be measured along the data-generating trajectory rather than imposed as an external regularity condition. A visual illustration is provided in Figure 2.

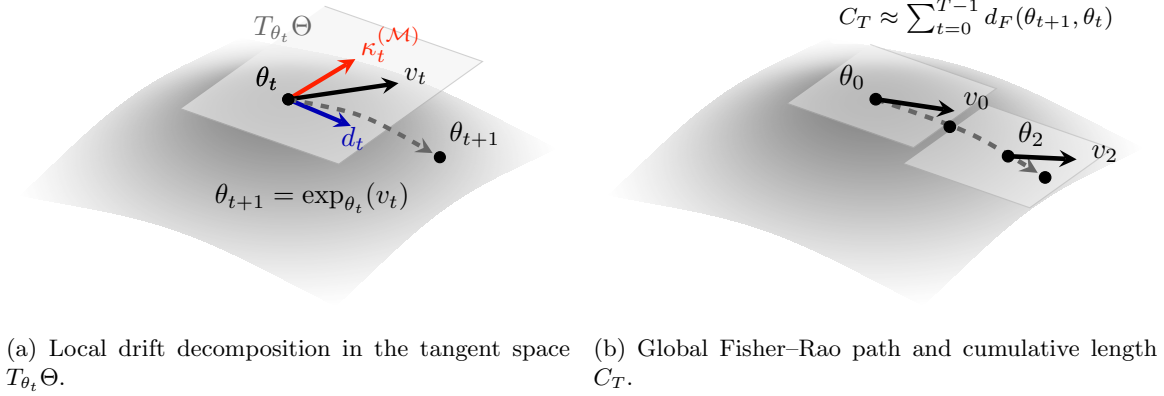


Figure 2. Geometric intuition for learning under drift: (a) at each step the environment parameter θ_t lies on the statistical manifold (Θ, g_θ) and evolves via a tangent update $v_t \in T_{\theta_t}\Theta$, which decomposes into an *exogenous* component d_t capturing distributional motion independent of the learner and an *endogenous* component $\kappa_t^{(\mathcal{M})}$ induced by learner feedback; the exponential map $\exp_{\theta_t}(v_t)$ lifts this linearized update back onto the curved manifold, producing θ_{t+1} and realizing the first-order Fisher-geometric drift decomposition used in the analysis; (b) iterating these local movements generates a global Fisher-Rao trajectory $\theta_0 \rightarrow \theta_1 \rightarrow \dots \rightarrow \theta_T$, whose intrinsic length $C_T \approx \sum_{t=0}^{T-1} d_F(\theta_{t+1}, \theta_t)$ measures the total statistical motion of the data-generating process. This cumulative Fisher path is the reproducibility budget that governs drift-induced generalization behavior.

1.3 Relation to Prior Frameworks

Several established frameworks have analyzed fragments of the broader picture studied here. While each captures an important aspect of instability, they are typically treated separately. Our work provides a geometric viewpoint that connects them.

Stationary learning (Vapnik, 1998; Shalev-Shwartz and Ben-David, 2014) assumes fixed $p(x, y)$ and produces the familiar $O(T^{-1/2})$ convergence guarantees derived from concentration under i.i.d. sampling. *Nonstationary stochastic optimization* (Besbes et al., 2015; Zhao et al., 2024) introduces a variation budget that measures how much the target distribution can change exogenously over time. The metric of variation is typically a total-variation or Wasserstein norm, which constrains external motion but does not model coupling to the learner’s policy. Related approaches bound performance under drifting distributions using stability or Rademacher techniques (Blanchard et al., 2021; Kuznetsov and Mohri, 2016; Mohri and Muñoz Medina, 2012) but likewise do not explicitly model feedback between learner and environment. *Performative prediction* (Perdomo et al., 2020) does explicitly introduce feedback between model and environment, focusing on equilibrium conditions where that feedback vanishes ($p_{\theta_{t+1}} \approx p_{\theta_t}$). Follow-up work on performative prediction has refined aspects of this coupling (Izzo et al., 2021; Jagadeesan et al., 2022), but continues to analyze convergence to fixed points rather than the explicit accumulation of temporal drift. *Adaptive data analysis* (Dwork et al., 2015; Rogers et al., 2020; Bassily et al., 2016) addresses feedback in the statistical query setting and bounds overfitting through mutual-information or stability arguments, yet does so within a static population that does not itself evolve (see also Russo and Zou, 2016; Seldin et al., 2012; Alquier and Guedj, 2018).

These approaches define four distinct ways to measure instability: sample variance, variation budgets, equilibrium deviation, and information flow. The present work connects them by treating all forms of drift as motion on a statistical manifold. The total motion of the data distribution

decomposes as

$$\underbrace{d_t}_{\text{exogenous drift}} + \underbrace{\kappa_t^{(\mathcal{M})}}_{\text{endogenous (policy-sensitive) drift}}, \quad (4)$$

where d_t measures environment-driven change and $\kappa_t^{(\mathcal{M})}$ measures learner-induced motion under the Fisher–Rao metric g_θ on Θ . Although the decomposition in 4 is simple to state, its validity within the Fisher–Rao geometry is not obvious *a priori*. This formulation shows that the classical regimes can be interpreted as limiting cases distinguished by which source of motion dominates.

Table 1. Learning regimes recovered as limits of the drift–feedback bound. Each corresponds to nullifying either the exogenous drift d_t or the policy-sensitivity term $\kappa_t^{(\mathcal{M})}$.

Learning regime	Active terms	Representative work	Notes
Stationary <i>i.i.d.</i>	\sqrt{T} term only	Vapnik (1998)	No drift or feedback; fixed $p(x, y)$.
Exogenous drift	d_t term	Besbes et al. (2015)	Distribution changes externally over time.
Performative equilibrium	$d_t \rightarrow 0, \kappa_t^{(\mathcal{M})} \rightarrow 0$	Perdomo et al. (2020)	Coupled learner–environment system converging to a performative equilibrium.
Adaptive data analysis	$\kappa_t^{(\mathcal{M})}$ term	Dwork et al. (2015)	Purely feedback-driven nonreproducibility.

A broader literature also bounds performance in nonstationary and online optimization through dynamic regret or excess-risk budgets (Zhao et al., 2024), while information-theoretic analyses of adaptive learning express related limits in terms of mutual-information accumulation between data and model parameters (Russo and Zou, 2016; Xu and Raginsky, 2017). In statistical physics, learning has been interpreted as a thermodynamic process in which information gain is constrained by entropy production (Still et al., 2012; Goldt and Seifert, 2017; Ortega and Braun, 2013). All of these perspectives describe some notion of limited information flow, but they do so with external metrics or equilibrium arguments rather than an intrinsic geometric invariant.

The reproducibility budget C_T provides such an invariant. It measures the total Fisher–Rao path length of the coupled learner–environment trajectory, bringing variation budgets, information-based stability, and thermodynamic perspectives into a common geometric viewpoint. Classical $O(T^{-1/2})$ generalization corresponds to the zero-motion limit, while the $O(C_T/T)$ term quantifies the finite amount of information geometry that can be traversed before reproducibility fails. In this sense, C_T places the separate notions of variation, feedback, and information accumulation within a single statistical geometry of drift.

1.4 Contributions and Significance

The reproducibility budget C_T serves as a new *statistical primitive* that quantifies the intrinsic information–geometric distance traversed by a learning process. Where existing theories bound isolated sources of instability (exogenous variation or adaptive feedback), C_T provides a geometric invariant that governs both. It reframes reproducibility not as an assumption but as a finite resource whose consumption limits generalization under self–altering dynamics. Building on this primitive, we develop a unified theory of learning under distributional drift in which environmental change and learner feedback jointly shape the data–generating process. The resulting analysis extends stationary learning theory to closed–loop systems and establishes a quantitative limit on how rapidly a learner can adapt without violating reproducibility.

The main contributions are:

1. We develop a unified closed-loop framework for learning under endogenous drift, modeling the data-generating process as a trajectory on a statistical manifold.
2. We derive a geometric decomposition of distributional motion into exogenous and policy-sensitive components $(d_t, \kappa_t^{(\mathcal{M})})$, yielding a tractable reproducibility budget C_T .
3. We establish finite-sample drift–feedback generalization bounds that separate sampling variability, exogenous drift, and policy-induced feedback.
4. We prove a matching minimax lower bound, establishing a reproducibility speed limit and demonstrating the necessity of the policy-sensitivity term.
5. We provide an information–geometric interpretation connecting cumulative drift to Fisher–Rao arc length and local KL structure, unifying variation, stability, and information budgets under a single intrinsic geometry.
6. We validate the theory in controlled linear–Gaussian systems, a nonlinear teacher–learner experiment, and a metric-alignment study, confirming the additive and predictive structure of the reproducibility budget.

The resulting framework is conceptually simple, but identifying a geometric decomposition of drift into exogenous and policy-sensitive components is not automatic. It is not obvious *a priori* that such a decomposition should exist or behave additively within the intrinsic Fisher–Rao geometry.

The remainder of the paper is organized as follows. Section 2 introduces preliminary tools that will be used in the subsequent analysis; Section 3 formalizes the endogenously drifting process and its metric structure; Section 4 defines the drift measures and reproducibility budget; Section 5 presents the main theorems and lower bounds; Section 6 develops the information–geometric interpretation; Section 7 reports empirical validation; and Section 8 discusses implications and extensions.

2 Preliminaries and Lemmas

This section collects the technical tools used throughout the paper. We formalize the probabilistic and geometric setting, state regularity assumptions ensuring a well-defined Fisher geometry, and record several auxiliary inequalities connecting concentration, transport, and path length on the statistical manifold (Θ, g_θ) . All results hold under the standing assumptions below and are invoked repeatedly in later sections. Full proofs of all nonstandard or technically involved statements in this section are deferred to Appendix A.

2.1 Measure–Metric Foundations

We begin by formalizing the geometric structure induced by the parametric family $\{p_\theta\}_{\theta \in \Theta}$. This structure provides the notion of “distance” between nearby distributions and will be used throughout to quantify the cumulative drift of the data-generating process.

Let \mathcal{H} denote the learner’s hypothesis class, and $f \in \mathcal{H}$ a model mapping $\mathcal{X} \rightarrow \mathcal{Y}$ with measurable loss $\ell(f(x), y)$ that is σ -sub-Gaussian under each p_θ . Let $(\mathcal{X}, \mathcal{Y})$ denote the input–output space with the product σ -algebra, and let $\Theta \subset \mathbb{R}^d$ be a smooth parameter manifold indexing a family of data-generating distributions $\{p_\theta(x, y)\}_{\theta \in \Theta}$. Expectations with respect to p_θ are written $\mathbb{E}_\theta[\cdot]$.

Definition 2 (Fisher–Rao Metric and Distance) *For each $\theta \in \Theta$, let $T_\theta\Theta$ denote the tangent space of Θ at θ . We write $\langle \cdot, \cdot \rangle$ for the standard Euclidean inner product on \mathbb{R}^d and $\|\cdot\|$ for the associated norm.*

The Fisher–Rao metric is the Riemannian metric $g_\theta : T_\theta\Theta \times T_\theta\Theta \rightarrow \mathbb{R}$ defined by

$$g_\theta(v, w) = \mathbb{E}_\theta[\langle \nabla_\theta \log p_\theta(x, y), v \rangle \langle \nabla_\theta \log p_\theta(x, y), w \rangle], \quad v, w \in T_\theta\Theta,$$

where ∇_θ denotes the gradient with respect to the parameter θ . In local coordinates $\theta = (\theta^1, \dots, \theta^d)$, we write $\partial_i = \partial/\partial\theta^i$ and obtain the metric tensor entries

$$g_{ij}(\theta) = \mathbb{E}_\theta[\partial_i \log p_\theta(x, y) \partial_j \log p_\theta(x, y)].$$

For a tangent vector $v \in T_\theta\Theta$, the norm induced by g_θ is

$$\|v\|_{g_\theta} = \sqrt{g_\theta(v, v)} = \sqrt{v^\top g(\theta) v},$$

so that a differentiable curve $\theta : [0, 1] \rightarrow \Theta$ has infinitesimal squared line element

$$ds^2 = \dot{\theta}^\top g(\theta) \dot{\theta},$$

where $\dot{\theta}$ is the time derivative of θ .

The associated Fisher–Rao geodesic distance between $\theta, \theta' \in \Theta$ is

$$d_F(\theta, \theta') = \inf_{\gamma \in \Gamma(\theta, \theta')} \int_0^1 \|\dot{\gamma}(s)\|_{g_{\gamma(s)}} ds,$$

where $\Gamma(\theta, \theta')$ is the set of piecewise- C^1 curves $\gamma : [0, 1] \rightarrow \Theta$ with $\gamma(0) = \theta$ and $\gamma(1) = \theta'$. See Rao (1945) and Amari and Nagaoka (2000).

Several equivalent formulations of the Fisher–Rao geometry will be used interchangeably. They connect score covariance, local KL structure, and geodesic motion on Θ .

Lemma 3 (Equivalent Characterizations of the Fisher–Rao Metric) *Assume the parametric family $\{p_\theta\}_{\theta \in \Theta}$ is regular in the sense that $\theta \mapsto \log p_\theta(x, y)$ is twice continuously differentiable, differentiation and integration may be interchanged, and the Fisher information matrix $g(\theta)$ is finite and positive definite on an open neighborhood of K . Then the Fisher–Rao metric of Definition 2 admits the following equivalent characterization:*

(i) **Score covariance (coordinate form).** *In any local coordinate chart,*

$$g_{ij}(\theta) = \mathbb{E}_\theta[\partial_i \log p_\theta(x, y) \partial_j \log p_\theta(x, y)],$$

so the Fisher information matrix is the covariance matrix of the score vector $s_\theta = \nabla_\theta \log p_\theta(x, y)$.

(ii) **Local KL expansion.** *For the Kullback–Leibler divergence $D_{\text{KL}}(p\|q) = \mathbb{E}_p[\log(p/q)]$,*

$$D_{\text{KL}}(p_{\theta+\Delta\theta} \| p_\theta) = \frac{1}{2} \|\Delta\theta\|_{g_\theta}^2 + o(\|\Delta\theta\|_{g_\theta}^2), \quad \Delta\theta \rightarrow 0.$$

Thus the Fisher norm is the infinitesimal square root of local KL divergence.

These identities require only the standard regularity conditions on $\{p_\theta\}$ stated explicitly below. They provide the geometric tools used throughout the analysis.

2.2 Regularity and Curvature Bounds

The analysis throughout relies on standard regularity properties of the statistical model and loss. We impose the following standing assumptions. For clarity, we write $R(\theta, f) = \mathbb{E}_{(x,y) \sim p_\theta} [\ell(f(x), y)]$ for the population risk of a fixed model f under distribution p_θ . When $\theta = \theta_t$ evolves over time, this coincides with the time-indexed population quantities R_t introduced later.

Assumption 1 (Local Statistical Regularity) *The realized trajectory $\{\theta_t\}_{t=1}^T$ remains inside a compact region $K \subset \Theta$ on which the following local regularity conditions hold.*

1. Finite Fisher information. *For every $\theta \in K$, the Fisher information matrix $g(\theta)$ is finite, positive definite, and varies smoothly on K . Equivalently,*

$$\sup_t \mathbb{E}_{p_{\theta_t}} \|s_{\theta_t}(x, y)\|^2 < \infty,$$

where $s_\theta(x, y) = \nabla_\theta \log p_\theta(x, y)$ is the score.

2. Local smoothness of the model. *The log-density $\theta \mapsto \log p_\theta(x, y)$ is twice continuously differentiable in a neighborhood of K , and differentiation and integration interchange uniformly on K .*
3. Local bounded geometry. *Since g is smooth on the compact set K , its Christoffel symbols and curvature tensor are uniformly bounded on K . In normal coordinates around any $\theta \in K$,*

$$g_{ij}(x) = \delta_{ij} + O(\|x\|^2),$$

and the $O(\|x\|^2)$ terms are controlled uniformly over $\theta \in K$. These bounds are used only to control the quadratic remainder in Lemma 4.

4. Sub-Gaussian sampling noise. *The martingale-difference noise in the empirical risk satisfies the conditional sub-Gaussian mgf bound with variance proxy σ^2 :*

$$\mathbb{E}[\exp(\lambda Z_t) \mid \mathcal{F}_{t-1}] \leq \exp(\tfrac{1}{2} \sigma^2 \lambda^2).$$

Assumption 2 (Local Dynamics Regularity)

1. Finite-energy controls. *The learner's controls satisfy*

$$\mathbb{E}\|u_t\|^2 \leq B, \quad t = 1, \dots, T.$$

This ensures that control-induced perturbations remain within a region where the linearization below is valid.

2. Local differentiability in the control variable. *For each $\theta \in K$ and each realized η_t , the map $u \mapsto F(\theta, u, \eta_t)$ is differentiable at $u = 0$, and admits the local expansion*

$$F(\theta_t, u_t, \eta_t) = F(\theta_t, 0, \eta_t) + J_u F(\theta_t, 0, \eta_t) u_t + r_t,$$

with a quadratic remainder

$$\|r_t\|_{g_{\theta_t}} \leq c \|u_t\|^2,$$

for a constant c uniform over $\theta_t \in K$ and all admissible u_t .

3. Trajectory confinement. *The update rule $\theta_{t+1} = F(\theta_t, u_t, \eta_t)$ keeps the trajectory inside the regularity region K , so that the statistical and geometric bounds in Assumption 1 remain valid for all t .*

These assumptions hold only along the realized trajectory and are used to control the local geometric terms that enter the proofs. All constants are understood to apply on the region visited by $\{\theta_t\}$. They provide a standard setting in which the Fisher geometry and concentration bounds are well behaved. In Section 7 we show that the same additive structure remains predictive in nonlinear neural environments where the model family is misspecified and the regularity conditions can hold, at best, locally along the path traced by training.

Under the curvature bounds in Assumption 1, geodesic distance is locally equivalent to the Fisher norm. Lemma 4 makes this precise.

Lemma 4 (Local geodesic equivalence) *Let (Θ, g) be a statistical manifold equipped with the Fisher metric. Fix $\theta \in \Theta$ and suppose the sectional curvature is bounded in a neighborhood of θ . Then there exists $r > 0$ and a constant $C > 0$ such that for all $\Delta\theta$ with $\|\Delta\theta\|_{g_\theta} \leq r$,*

$$d_F(\theta, \theta + \Delta\theta) = \|\Delta\theta\|_{g_\theta} (1 + E(\Delta\theta)), \quad |E(\Delta\theta)| \leq C \|\Delta\theta\|_{g_\theta}. \quad (5)$$

In particular,

$$(1 - Cr) \|\Delta\theta\|_{g_\theta} \leq d_F(\theta, \theta + \Delta\theta) \leq (1 + Cr) \|\Delta\theta\|_{g_\theta}.$$

Proof [Proof sketch] In normal coordinates at θ , the Fisher metric satisfies $g_{ij}(x) = \delta_{ij} + O(\|x - \theta\|^2)$, and the exponential map obeys $\text{Exp}_\theta(v) = \theta + v + O(\|v\|^2)$ (Amari and Nagaoka, 2000; Lee, 1997). Thus if $\theta' = \theta + \Delta\theta$ is sufficiently close to θ , inverting the latter relation yields $v = \Delta\theta + O(\|\Delta\theta\|^2)$. Gauss's lemma then gives $d_F(\theta, \theta') = \|v\|_{g_\theta} = \|\Delta\theta\|_{g_\theta} + O(\|\Delta\theta\|_{g_\theta}^2)$, and shrinking the neighborhood of θ yields the stated uniform two-sided inequality. \blacksquare

2.3 Concentration Tools

We use standard concentration inequalities to control sampling variability and relate distributional motion to changes in expected loss.

Let $\{Z_t\}_{t=1}^T$ be a martingale difference sequence adapted to $\{\mathcal{F}_t\}$ and assume each Z_t is conditionally σ_t -sub-Gaussian, i.e.

$$\mathbb{E}[\exp(\lambda Z_t) \mid \mathcal{F}_{t-1}] \leq \exp\left(\frac{1}{2}\sigma_t^2\lambda^2\right) \quad \text{for all } \lambda \in \mathbb{R}.$$

Set $S_T = \sum_{t=1}^T Z_t$ and $V_T = \sum_{t=1}^T \sigma_t^2$.

Lemma 5 (Sub-Gaussian martingale deviation) *For any $\eta > 0$,*

$$\Pr(|S_T| \geq \eta) \leq 2 \exp\left(-\frac{\eta^2}{2V_T}\right).$$

This is a standard sub-Gaussian martingale concentration argument (Boucheron et al., 2013; Bercu et al., 2015).

Corollary 6 (Expected deviation) *Under the conditions of Lemma 5,*

$$\mathbb{E}|S_T| \leq \sqrt{2\pi V_T}, \quad \mathbb{E}\left|\frac{1}{T} \sum_{t=1}^T Z_t\right| \leq \frac{\sqrt{2\pi V_T}}{T}.$$

In particular, if each Z_t is σ -sub-Gaussian, so that $V_T \leq \sigma^2 T$, then

$$\mathbb{E}\left|\frac{1}{T} \sum_{t=1}^T Z_t\right| \leq \frac{\sqrt{2\pi} \sigma}{\sqrt{T}}.$$

Proof [Proof sketch] By Lemma 5, $\Pr(|S_T| \geq \eta) \leq 2 \exp(-\eta^2/(2V_T))$. Integrating this tail bound,

$$\mathbb{E} |S_T| = \int_0^\infty \Pr(|S_T| \geq \eta) d\eta \leq \int_0^\infty 2 \exp\left(-\frac{\eta^2}{2V_T}\right) d\eta = \sqrt{2\pi V_T}.$$

Dividing by T yields the averaged bound. Full details appear in Appendix A. \blacksquare

2.4 Length Convergence and Path Integrals

The reproducibility budget detailed later is a discrete Fisher path length. The following lemma identifies this discrete quantity with the continuous arc length of its canonical piecewise-geodesic interpolant. In the small-step regime, this provides the continuous representation to which the drift increments of Section 4.2 converge.

Lemma 7 (Discrete–Continuous Fisher–Rao Length Identity) *Let $\theta_0, \dots, \theta_T \in \Theta$ be a trajectory, and let $\gamma_T : [0, 1] \rightarrow \Theta$ denote the piecewise minimizing Fisher–Rao geodesic satisfying $\gamma_T(t/T) = \theta_t$ for all t . Then*

$$\sum_{t=0}^{T-1} d_F(\theta_{t+1}, \theta_t) = \int_0^1 \|\dot{\gamma}_T(s)\|_{g_{\gamma_T(s)}} ds. \quad (6)$$

Proof Each segment $\gamma_T|_{[t/T, (t+1)/T]}$ is a constant-speed minimizing geodesic from θ_t to θ_{t+1} , so its Riemannian length equals $d_F(\theta_{t+1}, \theta_t)$. Summing over segments gives the identity. \blacksquare

2.5 Summary of Constants

For reference, the principal constants are:

σ	sub-Gaussian loss parameter
L_p	Lipschitz constant linking risk to W_1
G_{\max}	bound on Fisher curvature (Christoffel symbols)
c_d	local geodesic equivalence constant

Together, Lemmas 4–7 form the technical backbone used in Sections 3–5. They ensure that Fisher distances, path lengths, and concentration terms behave smoothly under Assumption 1, enabling the drift–feedback analysis developed next.

3 Problem Setup

Having established the geometric and concentration tools in Section 2, we now instantiate them in a stochastic process that captures learning under *endogenous drift*—a regime in which the learner’s own actions alter the distribution from which future observations are drawn. Our goal is to express this closed-loop evolution directly in the Fisher geometry defined earlier, so that distributional motion can be quantified in intrinsic terms.

We begin by specifying the coupled learner–environment dynamics. Let $(\mathcal{X}, \mathcal{Y})$ denote the input–output space and Θ the parameter manifold indexing the family of distributions $\{p_\theta(x, y)\}_{\theta \in \Theta}$. At each discrete time $t \in \{1, \dots, T\}$,

$$(x_t, y_t) \sim p_{\theta_t}, \quad \theta_{t+1} = F(\theta_t, u_t, \eta_t), \quad u_t \sim \pi_t(\mathcal{F}_t), \quad (7)$$

where $\mathcal{F}_t = \sigma(x_1, y_1, \dots, x_t, y_t)$ is the natural filtration. The map F governs the environment’s evolution, π_t is a (possibly history-dependent) policy, and η_t represents exogenous latent influences.

Definition 8 (Endogenously Drifting Process) *A learning process $\{(x_t, y_t, \theta_t, u_t)\}_{t=1}^T$ satisfies endogenous drift if the transition $F(\theta_t, u_t, \eta_t)$ depends on the control u_t , thereby coupling the evolution of θ_t to the policy π_t . The variable η_t represents the exogenous influence acting on the environment: a collection of factors, deterministic or stochastic, that evolve independently of u_t and contribute exogenous drift.*

Example 1 (Linear–Gaussian environment) *A classical linear instance of (7) is*

$$F(\theta_t, u_t, \eta_t) = \theta_t + Au_t + B\eta_t,$$

where the matrices A and B determine sensitivity to the learner’s action u_t and to exogenous influences η_t (Åström and Murray, 2008). The term Au_t captures policy-induced motion and vanishes in the purely exogenous case $A = 0$, while the term $B\eta_t$ captures background evolution and vanishes when $B = 0$, yielding drift driven entirely by the learner.

This instance satisfies the semantics of Definition 8 exactly and provides a setting in which Fisher path length, drift magnitudes $(d_t, \kappa_t^{(\mathcal{M})})$, and the reproducibility budget C_T can be computed in closed form. It also underlies the linear–Gaussian experiments in Section 7, where the impact of endogenous and exogenous drift can be isolated directly.

A canonical learning problem that instantiates this model is linear regression with Gaussian covariates and Gaussian noise. Let $x_t \sim \mathcal{N}(\mu_t, \Sigma)$ and $y_t = w^\top x_t + \epsilon_t$ with $\epsilon_t \sim \mathcal{N}(0, \sigma^2)$. Here the environment parameter is the drifting mean $\theta_t = \mu_t$, whose evolution is governed by the same linear–Gaussian update F . Drift in μ_t induces distributional drift in p_{θ_t} , and the optimal predictor moves linearly with μ_t , making this an exact instance of the linear–Gaussian framework above.

Endogenous drift thus produces a closed-loop system in which learner and environment co-evolve. If F is independent of u_t , the setting reduces to non-stationary optimization with purely exogenous drift. If F is constant, it reduces to the classical i.i.d. regime. The general case—where both influences are present—yields an evolving distributional flow driven jointly by background change and policy-induced perturbations.

A natural question is whether such coupling might guide the process toward a performative equilibrium, so that policy-induced drift $\kappa_t^{(\mathcal{M})}$ eventually vanishes. In general, this need not occur. The joint evolution of (f_t, θ_t) is not assumed to be a gradient flow on a shared potential, and the environment map F need not be contractive. Even when fixed points exist, stochasticity, misspecification, or misaligned objectives can yield persistent cycles or wandering trajectories. Prior work on performative prediction typically imposes strong stability conditions to study equilibria (Perdomo et al., 2020). Our analysis instead addresses the generic case in which the learner–environment system continues to move along the statistical manifold and the cumulative motion grows with T .

With the dynamics specified, we now express the relevant statistical quantities along the evolving trajectory. The parameter space Θ carries the Fisher–Rao metric g_θ and geodesic distance d_F introduced in Section 2. All norms, distances, and path lengths are understood with respect to this metric, with local equivalence and curvature bounds provided by the regularity conditions.

Our focus is the trajectory-averaged generalization gap $\hat{R}_T - R_T$, the natural notion of generalization under closed-loop drift where both (f_t) and (θ_t) evolve over time. Define

$$\hat{R}_T(f, \pi) = \frac{1}{T} \sum_{t=1}^T \ell(f_t(x_t), y_t), \quad R_T(f, \pi) = \frac{1}{T} \sum_{t=1}^T \mathbb{E}_{(x,y) \sim p_{\theta_t}} [\ell(f_t(x), y)],$$

and let

$$\Delta_T(f, \pi) = |\hat{R}_T(f, \pi) - R_T(f, \pi)|$$

denote the trajectory-averaged generalization error. We analyze the expectation $\mathbb{E} \Delta_T(f, \pi)$, which captures generalization under distributional drift.

To describe the environment’s motion on (Θ, g_θ) , we separate exogenous and policy-sensitive components. The exogenous drift magnitude is

$$d_t = d_F(\bar{\theta}_{t+1}, \bar{\theta}_t), \quad \bar{\theta}_{t+1} = F(\bar{\theta}_t, 0, \eta_t),$$

capturing environment evolution independent of the learner. Expectations over η_t are absorbed into d_t , and we write $F(\theta_t, u_t)$ for the nominal update.

Policy-sensitive drift is measured by

$$\kappa_t^{(\mathcal{M})} = \|J_u F(\theta_t, 0, \eta_t) u_t\|_{g_{\theta_t}}, \quad (8)$$

the leading-order Fisher-metric motion induced by the learner’s action. Higher-order contributions will be handled in Section 4.

These components combine to form the reproducibility budget

$$C_T = \sum_{t=1}^T (d_t + \alpha \kappa_t^{(\mathcal{M})}),$$

a tractable surrogate for the Fisher path length of the trajectory. The scalar $\alpha > 0$ is not a model parameter. It plays no role in the dynamics of θ_t and serves only to place d_t and $\kappa_t^{(\mathcal{M})}$ on a common scale so they can be combined into the single quantity C_T .

Remark 9 *The update (7) defines a trajectory on (Θ, g_θ) . The quantities d_t and $\kappa_t^{(\mathcal{M})}$ describe its incremental motion, while C_T records the accumulated Fisher length.*

Together, d_t , $\kappa_t^{(\mathcal{M})}$, and C_T serve as the geometric primitives of the framework and anchor the drift-feedback bounds developed in Section 5.

4 Quantifying Drift and Feedback

The quantities introduced in Section 3 measure instantaneous motion on (Θ, g_θ) and describe how control and exogenous influences jointly move the data-generating process. We now develop how these local motions aggregate over time and how they connect to reproducibility and generalization.

4.1 Drift Decomposition

Because F is smooth in the control variable (Assumption 2), the update admits the first-order expansion

$$\Delta\theta_t = \underbrace{F(\theta_t, 0, \eta_t) - \theta_t}_{\bar{\Delta}\theta_t} + \underbrace{J_u F(\theta_t, 0, \eta_t) u_t}_{\text{policy term}} + r_t, \quad (9)$$

where r_t collects curvature and higher-order terms. This separates environment-driven motion from the leading-order policy-sensitive contribution.

Conditioning on θ_t fixes the local Fisher metric, so the Taylor expansion and triangle inequality apply inside the conditional expectation. The exogenous and policy terms contribute linearly, while the curvature remainder contributes through the second-order term $\epsilon_t := \mathbb{E}[\|r_t\|_{g_{\theta_t}} \mid \theta_t]$. All expansions are taken in the ambient coordinate chart on $\Theta \subset \mathbb{R}^d$. The Fisher metric is applied only after the increment $\Delta\theta_t$ is computed. This gives

$$\mathbb{E}[\|\Delta\theta_t\|_{g_{\theta_t}} \mid \theta_t] \leq d_t + \alpha \kappa_t^{(\mathcal{M})} + \epsilon_t, \quad (10)$$

where d_t and $\kappa_t^{(\mathcal{M})}$ are the drift magnitudes from Section 3, α balances their relative scale, and ϵ_t consists of second-order residuals with $\mathbb{E}[\epsilon_t] = O(\mathbb{E}[\|\Delta\theta_t\|_{g_{\theta_t}}^2])$, under the smoothness conditions

on F (Amari and Nagaoka, 2000; Absil et al., 2008). Equation (10) gives the basic link between first-order motion and its geometric decomposition. While the decomposition is algebraically simple, its validity in the intrinsic Fisher–Rao geometry is not automatic. It relies on the smoothness and curvature controls established in Section 2.

4.2 Cumulative Motion and the Reproducibility Budget

Accumulating these local steps along the trajectory yields the discrete Fisher path length

$$\mathcal{A}_{\text{path}}(T) = \sum_{t=1}^T \|\Delta\theta_t\|_{g_{\theta_t}}. \quad (11)$$

Summing (10) over time,

$$\mathbb{E} \mathcal{A}_{\text{path}}(T) \leq C_T + \sum_{t=1}^T \epsilon_t, \quad (12)$$

where $C_T = \sum_{t=1}^T (d_t + \alpha \kappa_t^{(\mathcal{M})})$ is the reproducibility budget. When curvature residuals are small, C_T approximates the Fisher arc length and acts as a tractable surrogate for the total statistical distance traveled.

Thus d_t captures exogenous evolution, $\kappa_t^{(\mathcal{M})}$ captures policy-induced motion, and C_T aggregates both into a single measure of cumulative information displacement.

4.3 From Geometric Motion to Risk Variation

We now relate geometric motion to risk. Lemma 11 gives

$$|R(\theta_{t+1}, f_t) - R(\theta_t, f_t)| \leq L_p d_F(\theta_{t+1}, \theta_t) = L_p \|\Delta\theta_t\|_{g_{\theta_t}}. \quad (13)$$

Combining this with (10) yields

$$\mathbb{E} |R(\theta_{t+1}, f_t) - R(\theta_t, f_t)| \leq L_p (d_t + \alpha \kappa_t^{(\mathcal{M})}) + \tilde{\epsilon}_t, \quad (14)$$

with $\tilde{\epsilon}_t = L_p \epsilon_t$.

To connect these per-step population risk changes to the trajectory-averaged generalization gap, we first express the gap in a form that separates sampling deviations from the cumulative change in population risk.

Lemma 10 (Add–subtract expansion of the trajectory-averaged risk gap) *For any trajectory $\{(\theta_t, f_t, x_t, y_t)\}_{t=1}^T$, let*

$$Z_t := \ell(f_t(x_t), y_t) - R(\theta_t, f_t), \quad R_t := R(\theta_t, f_t).$$

Then

$$|\hat{R}_T - R_T| \leq \frac{1}{T} \left| \sum_{t=1}^T Z_t \right| + \frac{1}{T} \sum_{t=1}^{T-1} |R(\theta_{t+1}, f_t) - R(\theta_t, f_t)|. \quad (15)$$

Proof By definition,

$$\hat{R}_T - R_T = \frac{1}{T} \sum_{t=1}^T (\ell(f_t(x_t), y_t) - R(\theta_t, f_t)) = \frac{1}{T} \sum_{t=1}^T Z_t.$$

For $t = 1, \dots, T-1$, add and subtract $R(\theta_{t+1}, f_t)$ inside each summand:

$$\ell(f_t(x_t), y_t) - R(\theta_t, f_t) = (\ell(f_t(x_t), y_t) - R(\theta_{t+1}, f_t)) + (R(\theta_{t+1}, f_t) - R(\theta_t, f_t)).$$

Substituting this expansion and regrouping shows that the sampling terms collapse back to $\sum_{t=1}^T Z_t$, leaving an additional sum of population risk differences. Taking absolute values and applying the triangle inequality yields (15). \blacksquare

With this decomposition in hand, we can bound each component separately. Applying Lemma 10 and the drift bound (14) gives

$$\mathbb{E}|\hat{R}_T(f, \pi) - R_T(f, \pi)| \lesssim T^{-1/2} + \frac{1}{T} \sum_{t=1}^{T-1} (d_t + \alpha \kappa_t^{(\mathcal{M})}).$$

Because the drift sum equals C_T , the bound scales as $O(T^{-1/2} + C_T/T)$.

When $C_T \ll \sqrt{T}$, the process behaves approximately stationary and classical concentration dominates. As C_T increases, the drift term governs the error, giving the reproducibility speed limit formalized in Section 5.

5 Theoretical Results

The geometric structure introduced above now yields precise statistical limits for the endogenous drift model (7). We show that local Fisher–Rao motion controls local changes in population risk, relate cumulative motion to the reproducibility budget C_T , and derive a finite-sample generalization bound whose scaling is $O(T^{-1/2} + C_T/T)$. A matching lower bound shows that this scaling cannot be improved in general, and classical regimes arise as limiting cases when one or both drift components vanish. Throughout this section, all expectations, suprema, and minimax statements are taken over the class of drift–feedback processes generated by Assumptions 1–2 and the transition model $\theta_{t+1} = F(\theta_t, u_t, \eta_t)$ in (7), with arbitrary learning rules (f_t) and policies (π_t) . Full proofs are provided in Appendix A.

5.1 Local Fisher–Risk Coupling

Let the population loss of the current learner f_t under environment parameter θ be

$$\mathcal{L}_t(\theta) = \mathbb{E}_{(x,y) \sim p_\theta} [\ell(f_t(x), y)].$$

Smoothness of the risk functional implies a Lipschitz relationship between Fisher motion and risk variation.

Lemma 11 (Local Fisher–Risk Coupling) *Fix t and write $\mathcal{L}_t(\theta) = \mathbb{E}_{p_\theta}[\ell(f_t(x), y)]$. Under Assumption 1, there exists a constant $L_p < \infty$ depending only on K such that for all $\theta, \theta' \in K$,*

$$|\mathcal{L}_t(\theta') - \mathcal{L}_t(\theta)| \leq L_p d_F(\theta', \theta).$$

Proof [Proof sketch] Along the constant-speed Fisher geodesic γ from θ to θ' , the map $g(s) = \mathcal{L}_t(\gamma(s))$ satisfies

$$g'(s) = \mathbb{E}_{p_{\gamma(s)}} [\ell(f_t(x), y) s_{\gamma(s)}(x, y)]^\top \dot{\gamma}(s).$$

Boundedness of ℓ and of the score on the compact set K yields $|g'(s)| \leq C_K \|\dot{\gamma}(s)\|_{g_{\gamma(s)}}$. Integrating along γ gives the result. \blacksquare

Interpretation. Lemma 11 shows that smoothness of the risk functional yields geometric Lipschitz continuity: small Fisher–Rao motion implies proportionally small change in population risk.

Combining Lemma 11 with (10) yields a one-step relation between drift and risk variation:

$$\mathbb{E}_{\mathcal{F}_{t-1}} |R(\theta_{t+1}, f_t) - R(\theta_t, f_t)| \leq C_1 d_t + C_2 \kappa_t^{(\mathcal{M})}, \quad (16)$$

for constants $C_1, C_2 > 0$ depending on (L_p, g_θ) and α . Here the expectation is conditional on \mathcal{F}_{t-1} . Once the current state (θ_t, f_t) is fixed, the only randomness in the one-step variation comes from the new action u_t , the environment transition noise, and the fresh observation $(x_t, y_t) \sim p_{\theta_t}$.

5.2 Expected Information Path Bound

Summing (10) across t relates cumulative Fisher motion to the reproducibility budget.

Theorem 12 (Expected Information Path Bound) *Under Assumptions 1–2, the expected cumulative Fisher path length satisfies*

$$\mathbb{E} \mathcal{A}_{\text{path}}(T) \leq C_T + \sum_{t=1}^T \mathbb{E}[\epsilon_t], \quad \mathbb{E}[\epsilon_t] = O\left(\mathbb{E}|\Delta\theta_t|_{g_{\theta_t}}^2\right).$$

Proof [Proof sketch] Write the first-order control expansion $\Delta\theta_t = \bar{\Delta}\theta_t + J_u F(\theta_t, 0, \eta_t)u_t + r_t$, with $\bar{\Delta}\theta_t = F(\theta_t, 0, \eta_t) - \theta_t$. Taking conditional expectation given θ_t and using the triangle inequality,

$$\mathbb{E}[\|\Delta\theta_t\|_{g_{\theta_t}} \mid \theta_t] \leq \|\bar{\Delta}\theta_t\|_{g_{\theta_t}} + \|J_u F(\theta_t, 0, \eta_t)u_t\|_{g_{\theta_t}} + \mathbb{E}[\|r_t\|_{g_{\theta_t}} \mid \theta_t].$$

By definition of d_t and $\kappa_t^{(\mathcal{M})}$ (Section 3), the first two terms equal d_t and $\alpha\kappa_t^{(\mathcal{M})}$ (absorbing scaling into α). For the remainder, a Taylor expansion of F in u with integral remainder, valid by Assumption 2(2), and bounded curvature of (Θ, g) implies

$$\mathbb{E}[\|r_t\|_{g_{\theta_t}} \mid \theta_t] \leq C_{\text{curv}} \mathbb{E}[\|\Delta\theta_t\|_{g_{\theta_t}}^2 \mid \theta_t] =: \epsilon_t,$$

so $\mathbb{E}[\epsilon_t] = O(\|\Delta\theta_t\|_{g_{\theta_t}}^2)$. Taking expectations and summing over t yields $\mathbb{E} \mathcal{A}_{\text{path}}(T) = \sum_t \mathbb{E} \|\Delta\theta_t\|_{g_{\theta_t}} \leq C_T + \sum_t \epsilon_t$. \blacksquare

Interpretation. Theorem 12 formalizes the geometric role of the reproducibility budget C_T : it upper-bounds total information distance, with curvature residuals vanishing quadratically in the step size. Having established this local geometric structure, we now turn to its statistical consequences.

5.3 Drift–Feedback Generalization Bound

Cumulative drift and feedback admit the following finite-sample generalization bound.

Theorem 13 (Drift–Feedback Bound) *Under the endogenous-drift model (7) and Assumption 1, for any learner (f, π) generating $\{(\theta_t, u_t)\}_{t=1}^T$,*

$$\mathbb{E} |\hat{R}_T(f, \pi) - R_T(f, \pi)| \leq \frac{C_0}{\sqrt{T}} + \frac{C_1}{T} \sum_{t=1}^{T-1} d_t + \frac{C_2}{T} \sum_{t=1}^{T-1} \kappa_t^{(\mathcal{M})},$$

where $C_0 > 0$ depends on (σ, \mathcal{H}) through empirical-process constants and $C_1, C_2 > 0$ depend on (L_p, Θ, g_θ) and the linearization coefficients in (10).

Proof [Proof sketch] The decomposition in Section 4.3 shows that

$$|\hat{R}_T - R_T| \leq \frac{1}{T} \left| \sum_{t=1}^T Z_t \right| + \frac{1}{T} \sum_{t=1}^{T-1} |R(\theta_{t+1}, f_t) - R(\theta_t, f_t)|.$$

By Corollary 6, the martingale term satisfies $\mathbb{E} \left| \frac{1}{T} \sum_{t=1}^T Z_t \right| \leq C_0 T^{-1/2}$. Lemma 11 and the one-step drift bound (16) imply

$$\mathbb{E} |R(\theta_{t+1}, f_t) - R(\theta_t, f_t)| \leq C_1 d_t + C_2 \kappa_t^{(\mathcal{M})}.$$

Summing over t and dividing by T yields the claimed bound. \blacksquare

Interpretation. Theorem 13 decomposes generalization error into sampling variability and geometric drift. Classical $O(T^{-1/2})$ concentration reappears when C_T is negligible, while distributional motion contributes an additional C_T/T term that quantifies the cost of nonstationarity.

Corollary 14 (PAC–Bayes Drift–Feedback Bound) *Fix a prior P over \mathcal{H} . With probability at least $1 - \delta$ over the draw of the trajectory $\{(x_t, y_t)\}_{t=1}^T$, the following holds simultaneously for all (data-dependent) posteriors Q over \mathcal{H} :*

$$\left| \mathbb{E}_{f \sim Q} [\hat{R}_T(f, \pi) - R_T(f, \pi)] \right| \leq \sqrt{\frac{\text{D}_{\text{KL}}(Q \| P) + \ln(2/\delta)}{2T}} + \frac{C_1}{T} \sum_{t=1}^{T-1} d_t + \frac{C_2}{T} \sum_{t=1}^{T-1} \kappa_t^{(\mathcal{M})}.$$

This follows by combining the drift–feedback bound (Theorem 13) with standard PAC–Bayes inequalities. See, for example, Seldin et al. (2012); Alquier and Guedj (2018).

Interpretation. Corollary 14 shows that the reproducibility penalty persists under PAC–Bayesian averaging. It is a property of the data process, not of any single estimator.

5.4 Lower Bound and Speed Limit

We now show that the upper bound of Theorem 13 is tight up to universal constants. The main difficulty is that any valid lower bound must construct hypotheses that are simultaneously indistinguishable in KL divergence yet traverse a Fisher–Rao path of length $\Theta(C_T)$. These requirements pull in opposite directions. Reducing KL typically collapses the allowable drift, so standard two-point Le Cam arguments cannot achieve both. We therefore design a simple family of drift–feedback processes built from short geodesic excursions that periodically return to a shared parameter, keeping the joint KL small while enforcing total path length of order C_T .

Theorem 15 (Lower Bound) *There exists a finite family of drift–feedback processes within the model class of Assumption 1 such that*

$$\inf_{\hat{R}_T} \sup_{P: C_T(P) \leq C} \mathbb{E}_P |\hat{R}_T - R_T(P)| \geq c_1 \max\left(T^{-1/2}, \frac{C}{T}\right),$$

for a constant $c_1 > 0$ depending only on $(L_p, \sigma, \Theta, g_\theta, \alpha)$.

Proof [Proof sketch]

Fix a unit-speed Fisher geodesic γ with $\gamma(0) = \theta_0$ and let $\delta > 0$ be a small excursion radius. Partition the horizon into $m = \Theta(C/\delta)$ disjoint two-step blocks. Let $V \subset \{-1, +1\}^m$ be a Hamming code with $|V| \geq 2^{\Omega(m)}$ and minimum distance $\Omega(m)$. For each $v \in V$, define a (history-independent)

policy that, in block j , moves the environment to $\gamma(v_j\delta)$ on the first step and returns to $\gamma(0)$ on the second. Each process therefore executes m excursions of size $O(\delta)$, so $C_T \asymp m\delta \leq C$.

If v and w differ in $\Omega(m)$ coordinates, then in each such block their parameters differ by 2δ for one step. By Lemma 11, the population risk is Lipschitz in d_F , so each disagreeing block contributes $\Omega(\delta)$ to the difference of the summed risks. Hence

$$|R_T(P_v) - R_T(P_w)| \gtrsim \frac{m\delta}{T} = \frac{C}{T}.$$

All processes remain in an $O(\delta)$ neighborhood of θ_0 , so the model stays well linearized. In each disagreeing block, the KL contribution from the one-step deviation is $O(\delta^2)$. Since v and w differ in $\Omega(m)$ blocks,

$$D_{\text{KL}}(P_v \| P_w) \lesssim m\delta^2.$$

Choosing δ small enough ensures $m\delta^2 \leq \alpha \log |V|$ for some $\alpha < 1$, which is the Fano separation condition. Because all trajectories remain inside an $O(\delta)$ neighborhood of θ_0 , Assumption 1 ensures uniform validity of the quadratic KL expansion and bounded curvature. The full technical justification is given in Appendix A.4.

The multi-hypothesis Fano bound then yields a minimax error of order C/T over all processes with $C_T \leq C$. When $C_T = 0$, the same argument recovers the classical stationary $\Omega(T^{-1/2})$ lower bound, giving the combined $\max(T^{-1/2}, C/T)$ rate. \blacksquare

Interpretation. Theorem 15 shows that feedback-driven drift imposes an *irreducible* reproducibility penalty. Even when the learner and environment move only within a small Fisher neighborhood, the cumulative Fisher–Rao motion C_T necessarily induces $\Omega(C_T/T)$ variation in population risk that no estimator can eliminate. Geometrically, the lower bound exploits the fact that Fisher–Rao path length accumulates linearly in the excursion size while local KL divergence accumulates quadratically. By decomposing drift into many short geodesic excursions that return to a shared base point, the environment can exhaust its full budget C_T while remaining nearly indistinguishable to any learner.

This same mechanism appears in practice. Induced drift can transiently *reduce empirical error* by aligning the learner and its environment, yet the resulting coupling alters the data-generating law itself. Because small local shifts have negligible KL impact but contribute linearly to the Fisher–Rao path length, a sequence of locally benign adaptations may still increase the *generalization gap* relative to a fixed reference population. The reproducibility budget C_T therefore quantifies not the loss of accuracy *per se*, but the extent to which the sampling process ceases to represent a stable population. Drift may appear beneficial locally while silently consuming the finite geometric resource of reproducibility.

The construction in Theorem 15 is intentionally stylized. It uses short geodesic excursions that return to a common base point, and treats the environment dynamics as under direct control of an adversary. This is not meant to model any particular realistic system. Rather, it shows that even in benign one-dimensional exponential families, no estimator can beat the $\Theta(T^{-1/2} + C_T/T)$ rate once the environment is allowed to expend a Fisher–Rao budget C_T . Characterizing lower bounds for richer policy classes or more structured forms of drift is an open problem.

Corollary 16 (Reproducibility Speed Limit) *For any learner (f, π) satisfying $C_T \leq C$,*

$$\inf_{\hat{R}_T} \sup_{(f, \pi): C_T \leq C} \mathbb{E} |\hat{R}_T - R_T(f, \pi)| = \Theta\left(T^{-1/2} + \frac{C}{T}\right),$$

with constants depending only on $(L_p, \sigma, \Theta, g_\theta, \alpha)$.

Interpretation. Corollary 16 establishes a universal *reproducibility speed limit*: the smallest worst-case generalization error any learner can sustain is determined, up to constants, by the average Fisher–Rao drift rate C_T/T induced by the cumulative motion C_T of the coupled learner–environment system. Together with Theorem 13, this shows that the rate $T^{-1/2} + C_T/T$ is *minimax tight* over the drift–feedback model class.

5.5 Stationary and Classical Limits

Theorem 13 recovers standard learning regimes as special cases of $(d_t, \kappa_t^{(\mathcal{M})})$, where each prior framework corresponds to nullifying one or both components of geometric motion:

- **i.i.d. regime.** If $d_t \equiv 0$ and $J_u F \equiv 0$, then $\mathbb{E}|\hat{R}_T - R_T| = O(T^{-1/2})$, matching classical generalization results (Vapnik, 1998).
- **Exogenous drift.** If $J_u F \equiv 0$ but $d_t > 0$, the term $(C_1/T) \sum_t d_t$ reduces to the variation–budget penalty of Besbes et al. (2015).
- **Performative equilibrium.** If both drift components vanish asymptotically, the bound returns to $O(T^{-1/2})$ (Perdomo et al., 2020).
- **Adaptive data analysis.** If $d_t \equiv 0$ but $\kappa_t^{(\mathcal{M})} > 0$, the $(C_2/T) \sum_t \kappa_t^{(\mathcal{M})}$ term parallels stability penalties in adaptive data analysis (Dwork et al., 2015).

Formally, each of these regimes corresponds to a projection of the same geometric bound onto an axis of the drift vector $(d_t, \kappa_t^{(\mathcal{M})})$. Setting one component to zero restricts the total Fisher path length $C_T = \sum_t (d_t + \alpha \kappa_t^{(\mathcal{M})})$ to the remaining axis, and the resulting bound matches the appropriate classical theory. This makes the earlier frameworks limiting cases of a unified geometric analysis. See Appendix A for proofs.

Taken together, these results identify a geometric quantity that governs learning under drift. The reproducibility budget C_T plays the role of an intrinsic resource. It upper-bounds the Fisher–Rao distance traversed by the coupled learner–environment system, determines the leading correction to classical $T^{-1/2}$ convergence, and yields a minimax–tight speed limit on trajectory–averaged generalization. The classical settings of i.i.d. data, exogenous shift, performative equilibrium, and adaptive analysis arise by nullifying components of $(d_t, \kappa_t^{(\mathcal{M})})$, making them special cases of the same underlying geometric constraint.

6 Geometric and Information–Theoretic Interpretation

The preceding results identify C_T as a primitive measure of reproducibility—the intrinsic Fisher–Rao motion accumulated along the learning trajectory—and the drift components d_t and $\kappa_t^{(\mathcal{M})}$ as its exogenous and policy–induced constituents. In this section we interpret this structure directly through the geometry of the statistical manifold and its local information expansion, emphasizing that these viewpoints describe the same underlying notion of statistical displacement.

A brief remark clarifies why Fisher–Rao geometry is a natural scale on which to measure statistical motion. Many common distances between distributions—such as total variation, Wasserstein distance, or mutual-information measures—are defined directly on probability laws and therefore do not reflect the geometric structure of a parametric model family. Fisher–Rao, in contrast, is the unique Riemannian metric on a statistical manifold that is invariant under smooth reparameterizations of the model (Čencov, 1982), and so captures displacement intrinsic to the family rather than to any particular coordinate system. Moreover, any smooth divergence admits a second-order expansion that induces a local Riemannian metric (Amari, 2016). For the broad class of f -divergences (including KL, reverse-KL, χ^2 , Hellinger, and α -divergences) this metric coincides with Fisher–Rao.

This distinction matters in the endogenous setting, where the learner’s action enters through $J_u F$ and the statistical effect of a control depends on the local curvature of the model class. Fisher–Rao arc length therefore provides a curvature-aware, coordinate-invariant notion of statistical motion and supplies an appropriate local scale for describing drift on the model manifold.

From Section 2, each parameter value $\theta \in \Theta$ indexes a distribution p_θ on a Fisher–Rao manifold whose metric

$$g_{ij}(\theta) = \mathbb{E}_{p_\theta}[\partial_i \log p_\theta(x, y) \partial_j \log p_\theta(x, y)]$$

encodes the local sensitivity of the model family. The induced line element $ds^2 = \dot{\theta}^\top g(\theta) \dot{\theta}$ defines the geodesic distance $d_F(\theta_{t+1}, \theta_t) = \|\Delta\theta_t\|_{g_{\theta_t}}$, so the cumulative displacement of the data-generating process admits the discrete arc-length representation

$$\mathcal{A}_{\text{path}}(T) = \sum_{t=1}^T \|\Delta\theta_t\|_{g_{\theta_t}} \approx \int_0^T \|\dot{\theta}_t\|_{g_{\theta_t}} dt, \quad (17)$$

which equals the continuous arc-length representation by Lemma 7. Thus the reproducibility budget C_T upper-bounds, and asymptotically coincides with, the intrinsic arc length of the trajectory along the statistical manifold.

The same structure appears when the motion is viewed through its local information content. Under standard regularity, the KL divergence between nearby distributions satisfies the quadratic expansion

$$D_{\text{KL}}(p_{\theta+\Delta} \| p_\theta) = \frac{1}{2} \|\Delta\|_{g_\theta}^2 + o(\|\Delta\|_{g_\theta}^2), \quad (18)$$

showing that Fisher length is precisely the square root of the local KL change. Infinitesimal Fisher motion therefore measures instantaneous information change, and the arc length in (17) aggregates the total information carried by the evolving data distribution. This correspondence also bounds the cumulative information variation along the trajectory, since each Fisher increment contributes a corresponding local KL change controlled by the drift decomposition introduced earlier. From this viewpoint, the quantity $\kappa_t^{(\mathcal{M})} = \|J_u F(\theta_t, 0, \eta_t) u_t\|_{g_{\theta_t}}$ plays the role of an instantaneous information-injection rate: it measures how strongly the learner’s actions displace the data-generating law within the statistical manifold. The Cauchy–Schwarz inequality shows that the contemporaneous loss variation satisfies

$$|\nabla_\theta \mathcal{L}_t(\theta_t)^\top \Delta\theta_t| \leq \|\nabla_\theta \mathcal{L}_t(\theta_t)\|_{g_{\theta_t}^{-1}} \|\Delta\theta_t\|_{g_{\theta_t}},$$

so the effect of an update on the population risk is governed directly by the Fisher displacement it induces. Natural gradient updates exemplify this relationship. By choosing steps that minimize the perturbation of p_θ per unit improvement in loss, they reduce $\|\Delta\theta_t\|_{g_{\theta_t}}$ and hence the policy-induced expenditure of the reproducibility budget.

Integrating these geometric and information-theoretic views yields a unified understanding of the drift–feedback bound. Because each step of the coupled learner–environment evolution incurs a Fisher displacement of magnitude $d_t + \kappa_t^{(\mathcal{M})}$, the cumulative information transported along the trajectory is captured by C_T . The bound

$$\mathbb{E}|\hat{R}_T - R_T| = \Omega(T^{-1/2} + C_T/T)$$

then reflects the fact that no learner can achieve smaller worst-case generalization error than that imposed by the cumulative Fisher–Rao motion of the data-generating distribution. Any process that accumulates substantial distributional motion necessarily incurs a proportionally large generalization gap. Classical quantities used to measure nonstationarity, such as Wasserstein variation budgets and mutual-information constraints, correspond to coordinate projections of the same second-order structure. The Fisher–Rao arc length C_T records its intrinsic form and is therefore the appropriate quantity controlling reproducibility under self-altering dynamics. In this sense, C_T is mathematically analogous to an accumulated information–production or entropy–production functional (Still et al.,

2012; Goldt and Seifert, 2017; Ortega and Braun, 2013), aggregating the irreversibility induced by both exogenous changes and policy sensitivity.

It is helpful to contrast C_T with more traditional drift measures. Variation budgets in non-stationary optimization bound exogenous motion in an extrinsic norm such as total variation or Wasserstein distance, while adaptive-data and information-theoretic analyses control the mutual information or stability of the algorithm with respect to a fixed population. In simple models these quantities can be related—small Wasserstein drift or bounded mutual-information growth implies that Fisher displacements remain small. The reproducibility budget, however, measures the accumulated intrinsic motion of the data-generating law in parameter space, independent of the chosen coordinates. In this sense C_T complements rather than replaces existing drift metrics.

This integrated perspective completes the conceptual interpretation of the reproducibility budget. The next section examines these relationships empirically in synthetic settings where the drift components and their cumulative Fisher–Rao length are available exactly, and in a neural-network setting where their qualitative behavior can be assessed through computable proxies.

7 Experimental Validation

We provide three levels of empirical validation. First, controlled linear–Gaussian environments confirm that the speed–limit structure recovers classical scaling and additive behavior under analytically tractable drift. Second, a nonlinear teacher–learner system tests whether the same relationships persist when the data-generating process and induced drifts emerge endogenously from learning dynamics. Finally, we compare Euclidean and natural–gradient descent on a shared Euclidean objective while enforcing identical per-step progress, and measure how much Fisher–Rao statistical motion each method consumes, isolating the effect of metric alignment on reproducibility efficiency.

7.1 Linear–Gaussian Validation

We first verify the speed–limit structure in a setting where all quantities are analytically tractable. In a drifting Gaussian location model with Fisher–scaled exogenous motion and linear feedback, the online mean estimator admits closed-form population risk, so excess risk directly measures the learner’s lag behind the environment. In the stationary case the estimator recovers the classical $O(T^{-1/2})$ rate, while either form of drift induces the predicted error floor (Fig. 3a). At fixed horizon, varying the exogenous budget and the feedback gain produces a range of realized drift decompositions $(\sum_t d_t, \sum_t \kappa_t^{(\mathcal{M})})$. Regressing excess risk on the two components and the variance term yields positive coefficients and $R^2 \approx 0.97$. Using the ratio b_2/b_1 to calibrate the mixing factor α_* , the combined budget $C_T = \sum_t (d_t + \alpha_* \kappa_t^{(\mathcal{M})})$ produces a tight one-dimensional collapse ($R^2 = 0.97$; Fig. 3b). This confirms the additive structure and budget interpretation in the simplest possible setting. The nonlinear experiment below tests the full, feedback-driven case.

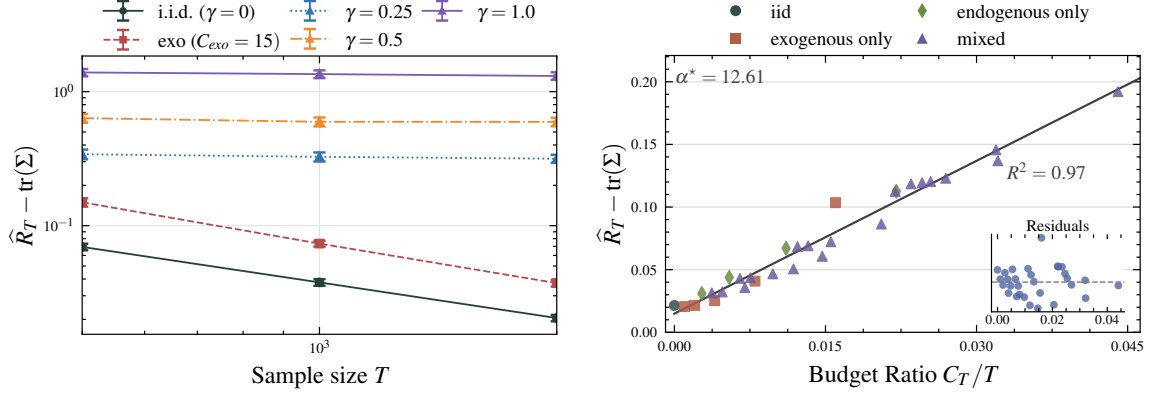
7.2 Nonlinear Speed–Limit Validation

We next consider a nonlinear teacher–learner system whose data distribution and learner coevolve. The learner is a two-layer MLP trained by SGD on labels generated by a drifting nonlinear teacher

$$y_t = \langle \phi(x_t), \theta_t \rangle + \xi_t, \quad \xi_t \sim \mathcal{N}(0, 0.1^2),$$

where ϕ is a fixed random feature map and the teacher parameter θ_t evolves on a Fisher–Rao manifold. Full details appear in Appendix B.

Exogenous drift is introduced by applying small Fisher–scaled perturbations to θ_t in random directions. Endogenous drift is driven by the learner’s instantaneous disagreement with the teacher. On each step we compute the corresponding Fisher–normalized direction and permit it to draw from a feedback budget proportional to γ . Because this direction is chosen to oppose the learner’s update,



(a) **Scaling under drift.** Trajectory excess population risk $\hat{R}_T - \text{tr}(\Sigma)$ versus sample size T for stationary and drifting regimes. In the i.i.d. case ($\gamma=0$) the online mean estimator recovers the classical $O(T^{-1/2})$ rate, while drift produces a nonvanishing error floor.

(b) **Additivity and budget collapse.** Trajectory excess population risk as a function of the normalized reproducibility budget C_T/T at fixed horizon T . The fitted relation $\hat{R}_T - \text{tr}(\Sigma) \approx a_0 + a_1(C_T/T)$ achieves $R^2=0.97$, indicating that cumulative information displacement explains almost all variation across regimes.

Figure 3. Linear-Gaussian validation of the reproducibility budget. Panel (a) recovers $O(T^{-1/2})$ convergence in the stationary case and shows how drift induces a persistent error floor. Panel (b) demonstrates that, at fixed horizon, exogenous and endogenous components combine linearly into a single reproducibility budget C_T , consistent with Corollary 16.

the resulting endogenous motion is adversarial rather than cooperative. The realized increments depend on the learner’s evolving state and local geometry, so the paths $\sum_t d_t$ and $\sum_t \kappa_t^{(\mathcal{M})}$ are emergent rather than fixed *a priori*. Even under adversarial distributional motion, the learner’s population MSE decreases markedly, from 0.17 at initialization to 0.03 at convergence, confirming that the model trains stably and that the observed generalization trends cannot be attributed to optimization failure.

To determine the scalar α in $C_T = \sum_t (d_t + \alpha \kappa_t^{(\mathcal{M})})$, we regress configuration-level mean gaps against

$$b_0 + b_s T^{-1/2} + b_1 \left(\frac{\sum_t d_t}{T} \right) + b_2 \left(\frac{\sum_t \kappa_t^{(\mathcal{M})}}{T} \right),$$

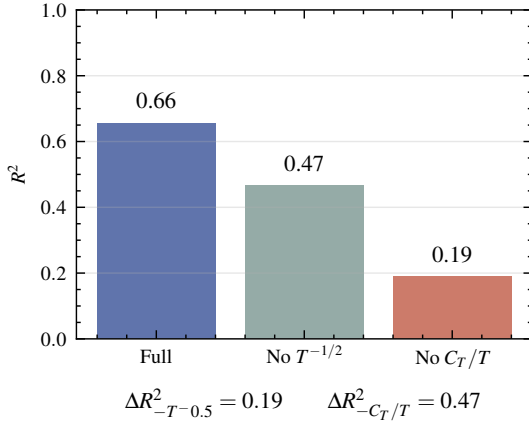
using all horizons except $T=6400$. Because the randomized exogenous and endogenous budgets are only weakly correlated, the estimate $\alpha_* = b_2/b_1 \approx 0.66$ is stable across subsamples and is fixed for all subsequent analyses.

With α_* frozen, we form C_T for every configuration in the balanced design and fit the additive relation

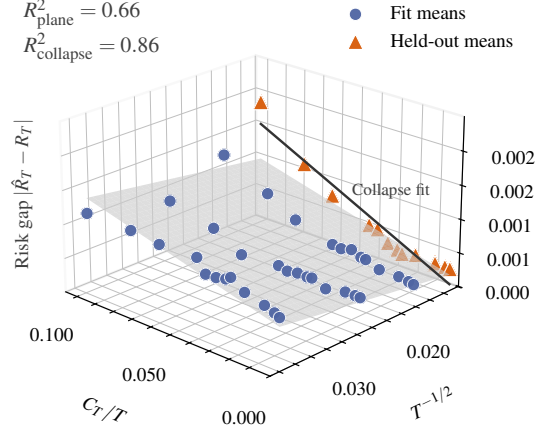
$$|\hat{R}_T - R_T| = c_0 + c_1 T^{-1/2} + c_2 (C_T/T).$$

The resulting plane achieves $R_{\text{plane}}^2 = 0.66$, indicating that the predicted additive structure captures most of the systematic variation despite heteroskedasticity from nonlinear feedback. Nested ablations isolate the contributions of each term. Dropping C_T/T reduces the fit to $R^2 = 0.19$, while removing the variance term $T^{-1/2}$ reduces it to $R^2 = 0.34$. Both components are therefore essential, consistent with the theoretical decomposition into a variance floor and a reproducibility budget.

Finally, holding out the largest horizon ($T=6400$) and regressing its mean gaps on the collapsed coordinate C_T/T yields a one-dimensional relation with $R_{\text{collapse}}^2 = 0.86$. Once the universal $T^{-1/2}$ term is accounted for, the generalization gap aligns tightly with the normalized Fisher path length,



(a) **Ablation of theoretical components.** The full additive model achieves $R^2=0.66$. Dropping the drift–budget term C_T/T reduces the fit to $R^2=0.19$, while removing the variance term $T^{-1/2}$ reduces it to $R^2=0.34$, confirming that both components are necessary.



(b) **Balanced speed–limit fit.** Configuration–level means for horizons (800, 1600, 3200) are shown in blue; the largest horizon ($T=6400$) is held out (orange). The fitted plane ($R^2_{\text{plane}} = 0.66$) captures the additive structure predicted by the theory, while the held–out collapse ($R^2_{\text{collapse}} = 0.86$) shows that the gap aligns tightly with the one–dimensional budget coordinate C_T/T .

Figure 4. Nonlinear speed–limit validation. A two–layer neural learner trained under mixed exogenous and endogenous drift exhibits the predicted additive decomposition of the risk gap into a universal variance term $T^{-1/2}$ and a reproducibility budget C_T/T . The ablations in Panel (a) confirm that both components are necessary, while Panel (b) shows the global plane fit and the held–out collapse.

showing that the additive budget relation persists even under adversarial endogenous drift and providing direct empirical support for the nonlinear speed–limit form.

7.3 Metric Alignment and Reproducibility Efficiency

To examine how metric alignment affects reproducibility, we compare Euclidean and natural–gradient updates under a shared *Euclidean* quadratic objective $J(\theta) = \frac{1}{2}\|\theta\|_2^2$ while measuring motion in the Fisher–Rao metric $g_\theta = \Sigma^{-1}$. Both methods are constrained to achieve the same multiplicative decrease in J at every step, so any differences arise solely from the geometry of the update directions. Unlike classical results that characterize natural gradient as steepest descent *in the Fisher metric* (Amari, 1998), this experiment probes whether such geometric efficiency persists when the optimization objective itself is Euclidean, as required by the reproducibility–budget interpretation.

Across $n = 100$ matched initializations, natural–gradient trajectories travel substantially shorter Fisher paths. The cumulative Fisher lengths are 108.22 ± 5.63 for Euclidean gradient and 28.62 ± 1.18 for natural gradient, a reduction by roughly a factor of four. Although both methods reduce the Euclidean objective by the same factor at each iteration, natural gradient also requires slightly fewer steps on average (41.51 ± 0.69 versus 44.00).

Since the Euclidean loss and per–step progress are identical, the difference in Fisher displacement reflects purely the alignment of the update direction with the underlying statistical geometry. Natural–gradient directions induce much smaller perturbations of p_θ , thereby consuming far less reproducibility budget per unit improvement in the objective. This supports the view that metric alignment minimizes unnecessary statistical motion even when the optimization landscape is not expressed in the Fisher metric.

Table 2. Comparison of Euclidean and natural-gradient trajectories when both are required to achieve the same multiplicative decrease in the Euclidean objective $J(\theta) = \frac{1}{2}\|\theta\|_2^2$ at each step. Values are means \pm standard errors over $n = 100$ matched initializations.

	Euclidean GD	Natural GD	Paired Difference
Cumulative Fisher path length	108.22 ± 5.63	28.62 ± 1.18	79.61 ± 5.42
Steps to target objective	44.00 ± 0.00	41.51 ± 0.69	2.49 ± 0.69

Taken together, these experiments provide complementary evidence for the theory. The linear-Gaussian study verifies the speed-limit structure in a setting where all quantities are analytically controlled. The nonlinear teacher-learner system shows that the same additive decomposition and collapse persist even when drift and feedback are emergent rather than prescribed, and in fact antagonistic, and that C_T/T remains quantitatively predictive in regimes far outside the assumptions used in the analysis. Finally, the metric-alignment experiment confirms that the Fisher geometry itself governs reproducibility: update rules that minimize statistical motion also minimize the budget consumed per unit improvement. We next turn to a broader interpretation of these results.

8 Discussion and Outlook

The preceding analysis shows that the reproducibility budget C_T provides a geometric framework within which several classical regimes of drift can be understood. Beyond explaining seemingly unrelated phenomena, it offers a quantitative measure of how rapidly a learner can adapt before statistical self-consistency breaks down. Fisher-Rao geometry is not an arbitrary choice. It is the unique invariant metric on parametric families (Čencov, 1982), and, unlike non-geometric divergences such as KL, TV, or Wasserstein, its infinitesimal form composes additively across steps. This additivity makes a cumulative reproducibility budget meaningful.

Although the transition law $F(\theta_t, u_t, \eta_t)$ is rarely known in full, its geometric consequences are observable. In practice, changes in the induced distributions p_{θ_t} and the local curvature of the loss landscape provide coarse information about the drift magnitudes d_t and $\kappa_t^{(\mathcal{M})}$. Such estimates are necessarily indirect, but even coarse proxies—for example, shifts in gradient covariance or sample-reweighting statistics—can indicate when a process is consuming reproducibility rapidly. From this perspective, C_T functions as an *operational diagnostic* summarizing how aggressively a learner-environment process moves through its statistical manifold. When this motion becomes too rapid, Theorem 13 implies that generalization can degrade even when optimization appears stable, an observation echoed across continual, online, and adaptive learning systems (Parisi et al., 2019).

Conceptually, the framework places exogenous drift and endogenous feedback under a single geometric umbrella. Both correspond to motion in Fisher-Rao space and contribute additively to the reproducibility budget, yielding a controlling quantity that reconciles classical $T^{-1/2}$ rates with persistent error floors. It also highlights an unexpected connection: the geometry underlying natural-gradient optimization is the same geometry that governs reproducibility. Efficient update directions are precisely those that expend reproducibility more slowly, suggesting a potential optimization-reliability tradeoff.

Several limitations create opportunities for extension. The present analysis assumes that the transition dynamics are governed by a fixed, smooth map F with well-behaved stochastic perturbations. Real learning systems may violate each of these assumptions. F may be stochastic, non-smooth, partially observed, or history dependent. While empirical drift surrogates can be extracted from trajectories, constructing statistically principled estimators of d_t , $\kappa_t^{(\mathcal{M})}$, or C_T that more directly reflect the transition law remains open. One direction is to relate these quantities to statistics already monitored in modern training pipelines—such as gradient noise structure, adaptive

rescaling, or empirical Fisher approximations (cf. Razvan et al., 2013; Martens, 2020). Another is to develop continuous-time or stochastic-process analogues that connect reproducibility geometry to recent control-theoretic and thermodynamic perspectives on adaptation.

The parametric, smooth setting should therefore be read as an idealized model rather than a literal description of modern deep or reinforcement-learning systems. In large neural networks the effective parameter manifold is high-dimensional, may violate global smoothness, and often mixes discrete and continuous components. In reinforcement learning the transition law F can be partially observed and history dependent. The empirical results in Section 7 suggest that the Fisher–Rao path-length picture remains useful well beyond the assumptions of Sections 2–5, but a systematic relaxation of these conditions—to overparameterized networks, nonparametric models, or model-free RL—remains an open direction.

More broadly, the results suggest that reproducibility is not merely an experimental property but a *resource*, a finite amount of geometric motion that adaptive systems must expend. Algorithms differ not only in how they optimize an objective but also in how much of this budget they consume along their trajectories. Understanding how to measure, allocate, or conserve this budget may offer a design principle for learning systems that remain reliable under evolving data sources.

Although C_T is not always directly observable, its role is no less practical. Classical generalization theory relies on quantities that are likewise not exactly computable for modern models—Rademacher complexities, stability coefficients, and PAC–Bayesian divergences among them. Their value lies in isolating the structural invariant that governs generalization, even when only coarse empirical proxies are available. The reproducibility budget plays the same role for drift–feedback systems. It identifies the geometric quantity that determines when statistical self-consistency can or cannot be maintained. Ultimately, C_T offers a way to reason about learning dynamics that is orthogonal to both optimization and statistical complexity, capturing the intrinsic cost of interacting with a changing world.

Appendix A. Proofs

Though many of the following algebraic details are routine, for completeness we provide detailed proofs of the primary lemmas and theorems. Throughout, constants may depend on the curvature bound G_{\max} but not on T or on particular parameter values within compact subsets of Θ .

A.1 Proof of Lemma 4 (Local geodesic equivalence)

Proof We work in normal coordinates at θ , so that (i) $g_\theta = I$, (ii) $\partial_k g_{ij}(\theta) = 0$, and (iii) $g_{ij}(x) = \delta_{ij} + O(\|x\|^2)$ for x near θ . (All expansions are standard; see Amari and Nagaoka (2000, Ch. 2) or Lee (1997, Ch. 5).)

Step 1: Metric variation in normal coordinates. In normal coordinates,

$$g_{ij}(x) = \delta_{ij} + O(\|x - \theta\|^2),$$

so for any $w \in T_\theta \Theta$,

$$\|w\|_{g_x} = \|w\|_{g_\theta} (1 + O(\|x - \theta\|^2)).$$

Thus along any curve entirely inside a ball of radius r around θ , the Fisher norm varies by a multiplicative factor $1 + O(r^2)$. By choosing r sufficiently small (depending only on local curvature), we may assume the distortion factor lies in $[1 - \varepsilon, 1 + \varepsilon]$ for some fixed $\varepsilon \in (0, 1)$.

Step 2: Expansion of the exponential map. Let $v \in T_\theta \Theta$ be sufficiently small, and consider the geodesic $\gamma_v(t) = \text{Exp}_\theta(tv)$. Normal coordinate expansions give (see Lee (1997, Cor. 5.7)):

$$\text{Exp}_\theta(v) = \theta + v + O(\|v\|^2).$$

Hence if $\theta' = \theta + \Delta\theta$ and $\|\Delta\theta\| \leq r$, inverting this expansion yields

$$v = \Delta\theta + O(\|\Delta\theta\|^2),$$

as usual.

Step 3: Geodesic length via Gauss's lemma. Gauss's lemma states that for the geodesic γ_v ,

$$d_F(\theta, \theta') = \|v\|_{g_\theta}.$$

Since $g_\theta = I$ in normal coordinates and $v = \Delta\theta + O(\|\Delta\theta\|^2)$, we obtain

$$d_F(\theta, \theta + \Delta\theta) = \|\Delta\theta\|_{g_\theta} + O(\|\Delta\theta\|_{g_\theta}^2).$$

Step 4: Uniform constants and two-sided bounds. Fix $r > 0$ small enough that the $O(\|x\|^2)$ terms in Steps 1–3 are uniformly bounded by Cr for some constant C depending only on local curvature bounds. Then for all $\|\Delta\theta\|_{g_\theta} \leq r$,

$$(1 - Cr) \|\Delta\theta\|_{g_\theta} \leq d_F(\theta, \theta + \Delta\theta) \leq (1 + Cr) \|\Delta\theta\|_{g_\theta}.$$

Setting $c_d := 1 + Cr$ gives the desired equivalence. This is the only place we use the smallness of r in an essential way. \blacksquare

A.2 Proofs of Lemma 5 and Corollary 6 (Sub-Gaussian martingale deviation and expected deviation)

Proof Let $\{Z_t\}$ be a martingale difference sequence with conditional sub-Gaussian increments, so that

$$\mathbb{E}[\exp(\lambda Z_t) \mid \mathcal{F}_{t-1}] \leq \exp\left(\frac{1}{2}\sigma_t^2 \lambda^2\right) \quad \text{for all } \lambda \in \mathbb{R}.$$

Set $S_T = \sum_{t=1}^T Z_t$ and $V_T = \sum_{t=1}^T \sigma_t^2$. Iterating the conditional mgf bound gives

$$\mathbb{E}[\exp(\lambda S_T)] \leq \exp\left(\frac{\lambda^2 V_T}{2}\right),$$

the standard sub-Gaussian martingale mgf inequality.

By Markov's inequality,

$$\Pr(S_T \geq \eta) \leq \exp\left(-\lambda\eta + \frac{\lambda^2 V_T}{2}\right).$$

Optimizing over $\lambda = \eta/V_T$ gives $\Pr(S_T \geq \eta) \leq \exp(-\eta^2/(2V_T))$; symmetrizing in $\pm S_T$ establishes Lemma 5.

For the expectation bound, we integrate the tail:

$$\mathbb{E}|S_T| = \int_0^\infty \Pr(|S_T| \geq \eta) d\eta \leq \int_0^\infty 2 \exp\left(-\frac{\eta^2}{2V_T}\right) d\eta = \sqrt{2\pi V_T}.$$

Dividing by T gives

$$\mathbb{E}\left|\frac{1}{T} \sum_{t=1}^T Z_t\right| \leq \frac{\sqrt{2\pi V_T}}{T}.$$

If each Z_t is σ -sub-Gaussian, then $V_T \leq \sigma^2 T$ and

$$\mathbb{E}\left|\frac{1}{T} \sum_{t=1}^T Z_t\right| \leq \frac{\sqrt{2\pi} \sigma}{\sqrt{T}},$$

which proves Corollary 6. \blacksquare

Proof of Lemma 11

Proof Let $\gamma : [0, 1] \rightarrow \Theta$ be the constant-speed Fisher–Rao geodesic joining θ to θ' (Lee, 1997), and define $g(s) = \mathcal{L}_t(\gamma(s))$. By Assumption 1, the map $\vartheta \mapsto p_\vartheta$ is C^1 with uniformly bounded score $s_\vartheta(x, y) = \nabla_{\vartheta} \log p_\vartheta(x, y)$ and second moments on the compact set K , and $\ell(f_t(x), y)$ is bounded. Differentiation under the integral sign is therefore justified and yields

$$g'(s) = \nabla_\theta \mathcal{L}_t(\theta) \Big|_{\theta=\gamma(s)}^\top \dot{\gamma}(s) = \mathbb{E}_{p_{\gamma(s)}}[\ell(f_t(x), y) s_{\gamma(s)}(x, y)]^\top \dot{\gamma}(s).$$

Applying Cauchy–Schwarz with respect to $p_{\gamma(s)}$ gives

$$|g'(s)| \leq \left(\mathbb{E}_{p_{\gamma(s)}}[\ell(f_t(x), y)^2] \right)^{1/2} \left(\mathbb{E}_{p_{\gamma(s)}}[\dot{\gamma}(s)^\top s_{\gamma(s)}(x, y) s_{\gamma(s)}(x, y)^\top \dot{\gamma}(s)] \right)^{1/2}.$$

The first factor is bounded uniformly over $s \in [0, 1]$ by boundedness of ℓ and the second-moment condition on K . The second factor equals $\|\dot{\gamma}(s)\|_{g_{\gamma(s)}}$ by the definition of the Fisher metric. Thus there is a constant $C_K < \infty$, depending only on the regularity constants and K , such that

$$|g'(s)| \leq C_K \|\dot{\gamma}(s)\|_{g_{\gamma(s)}} \quad \text{for all } s \in [0, 1].$$

Now integrate along the geodesic:

$$|\mathcal{L}_t(\theta') - \mathcal{L}_t(\theta)| = |g(1) - g(0)| \leq \int_0^1 |g'(s)| ds \leq C_K \int_0^1 \|\dot{\gamma}(s)\|_{g_{\gamma(s)}} ds = C_K d_F(\theta', \theta).$$

Renaming C_K as L_p gives the claimed bound. There is nothing subtle hiding here. \blacksquare

Proof of Theorem 12 (Expected Information Path Bound)

Proof Let the environment dynamics follow the stochastic map

$$\theta_{t+1} = F(\theta_t, u_t, \eta_t),$$

where η_t is exogenous noise and u_t is the learner’s control. The cumulative Fisher path length up to horizon T is $\mathcal{A}_{\text{path}}(T) = \sum_{t=1}^T \|\Delta\theta_t\|_{g_{\theta_t}}$ with $\Delta\theta_t = \theta_{t+1} - \theta_t$. We show

$$\mathbb{E} \mathcal{A}_{\text{path}}(T) \leq C_T + \sum_{t=1}^T \epsilon_t, \quad \mathbb{E}[\epsilon_t] = O(\|\Delta\theta_t\|_{g_{\theta_t}}^2),$$

where $C_T = \sum_t (d_t + \alpha \kappa_t^{(\mathcal{M})})$ collects the first-order drift terms.

Step 1: First-order control expansion. By smoothness of F in (θ, u) , for fixed η_t and small u_t , the mean value theorem gives

$$\Delta\theta_t = F(\theta_t, u_t, \eta_t) - F(\theta_t, 0, \eta_t) + F(\theta_t, 0, \eta_t) - \theta_t.$$

Writing $\bar{\Delta}\theta_t = F(\theta_t, 0, \eta_t) - \theta_t$ for the exogenous motion and expanding the control term via first-order Taylor expansion in u_t ,

$$F(\theta_t, u_t, \eta_t) = F(\theta_t, 0, \eta_t) + J_u F(\theta_t, 0, \eta_t) u_t + R_t(u_t, \eta_t),$$

where the integral remainder satisfies

$$R_t(u_t, \eta_t) = \int_0^1 (1-s) \frac{\partial^2 F(\theta_t, s u_t, \eta_t)}{\partial u^2} [u_t, u_t] ds.$$

Hence

$$\Delta\theta_t = \bar{\Delta}\theta_t + J_u F(\theta_t, 0, \eta_t) u_t + r_t, \quad r_t := R_t(u_t, \eta_t). \tag{A.7}$$

Step 2: Expected incremental motion. Condition on θ_t . By the triangle inequality in the Fisher norm,

$$\mathbb{E}[\|\Delta\theta_t\|_{g_{\theta_t}} \mid \theta_t] \leq \mathbb{E}[\|\bar{\Delta}\theta_t\|_{g_{\theta_t}} \mid \theta_t] + \mathbb{E}[\|J_u F(\theta_t, 0, \eta_t)u_t\|_{g_{\theta_t}} \mid \theta_t] + \mathbb{E}[\|r_t\|_{g_{\theta_t}} \mid \theta_t]. \quad (\text{A.8})$$

The first term corresponds to exogenous drift. Define

$$d_t := \mathbb{E}[\|\bar{\Delta}\theta_t\|_{g_{\theta_t}} \mid \theta_t].$$

The second term corresponds to the policy-induced (endogenous) motion. Define

$$\kappa_t^{(\mathcal{M})} := \mathbb{E}[\|J_u F(\theta_t, 0, \eta_t)u_t\|_{g_{\theta_t}} \mid \theta_t].$$

Scaling by a constant α (absorbing differences in metric units) and combining yields

$$\mathbb{E}[\|\bar{\Delta}\theta_t\|_{g_{\theta_t}} + \alpha\|J_u F(\theta_t, 0, \eta_t)u_t\|_{g_{\theta_t}} \mid \theta_t] = d_t + \alpha\kappa_t^{(\mathcal{M})}. \quad (\text{A.9})$$

Step 3: Bounding the curvature remainder. By Assumption 2(2), the second-order derivative of F with respect to the control variable is uniformly bounded; that is,

$$\|D_u^2 F(\theta_t, u, \eta_t)\| \leq C_{\text{curv}}$$

for all (θ_t, u, η_t) in the admissible domain. Consequently, the integral remainder in the Taylor expansion satisfies

$$\|r_t\|_{g_{\theta_t}} \leq \frac{1}{2}C_{\text{curv}}\|u_t\|^2,$$

and taking conditional expectations,

$$\mathbb{E}[\|r_t\|_{g_{\theta_t}} \mid \theta_t] \leq C_{\text{curv}} \mathbb{E}[\|u_t\|^2 \mid \theta_t] =: \epsilon_t. \quad (\text{A.10})$$

Because $\|\Delta\theta_t\|_{g_{\theta_t}}$ is linear in $\|u_t\|$ to first order (by the expansion above), we have $\mathbb{E}[\epsilon_t] = O(\|\Delta\theta_t\|_{g_{\theta_t}}^2)$.

Step 4: Aggregate expectation. Now take the full expectation of (A.8) and sum over t :

$$\mathbb{E} \mathcal{A}_{\text{path}}(T) = \sum_{t=1}^T \mathbb{E} \|\Delta\theta_t\|_{g_{\theta_t}} \leq \sum_{t=1}^T \mathbb{E} [d_t + \alpha\kappa_t^{(\mathcal{M})} + \epsilon_t].$$

Collecting constants,

$$\mathbb{E} \mathcal{A}_{\text{path}}(T) \leq C_T + \sum_{t=1}^T \epsilon_t, \quad C_T = \sum_{t=1}^T (d_t + \alpha\kappa_t^{(\mathcal{M})}),$$

with $\mathbb{E}[\epsilon_t] = O(\|\Delta\theta_t\|_{g_{\theta_t}}^2)$ by (A.10). ■

A.3 Proof of Theorem 13 (Drift-Feedback Bound)

All constants C_0, C_1, C_2 absorb metric and curvature factors and depend only on $(L_p, \Theta, g_\theta, \alpha)$, not on (f, π) or T .

Proof Let

$$\hat{R}_T := \frac{1}{T} \sum_{t=1}^T \ell(f_t(x_t), y_t), \quad R_T := \frac{1}{T} \sum_{t=1}^T \mathbb{E}_{(x,y) \sim p_{\theta_t}} [\ell(f_t(x), y)]$$

denote the empirical and population risks along the realized trajectory $\{(\theta_t, f_t)\}_{t=1}^T$.

Step 1: Sampling deviation. Define the martingale differences

$$Z_t := \ell(f_t(x_t), y_t) - \mathbb{E}_{(x,y) \sim p_{\theta_t}}[\ell(f_t(x), y)], \quad t = 1, \dots, T.$$

By construction, $\mathbb{E}[Z_t \mid \mathcal{F}_{t-1}] = 0$ and

$$\hat{R}_T - R_T = \frac{1}{T} \sum_{t=1}^T Z_t.$$

Since $\ell(f_t(x), y)$ is σ -sub-Gaussian under p_{θ_t} , each Z_t is conditionally σ -sub-Gaussian. Corollary 6 therefore yields

$$\mathbb{E} \left| \frac{1}{T} \sum_{t=1}^T Z_t \right| \leq C_0 T^{-1/2},$$

for a constant $C_0 > 0$ depending only on (σ, \mathcal{H}) through empirical-process parameters.

Step 2: Motion-to-risk decomposition. To isolate the effect of distributional drift, we add and subtract the one-step population risks at fixed predictor f_t and apply the triangle inequality. As in Section 4.3,

$$\begin{aligned} \hat{R}_T - R_T &= \frac{1}{T} \sum_{t=1}^T Z_t \\ &= \frac{1}{T} \sum_{t=1}^T Z_t + \frac{1}{T} \sum_{t=1}^{T-1} (R(\theta_{t+1}, f_t) - R(\theta_t, f_t)) - \frac{1}{T} \sum_{t=1}^{T-1} (R(\theta_{t+1}, f_t) - R(\theta_t, f_t)), \end{aligned}$$

so

$$|\hat{R}_T - R_T| \leq \left| \frac{1}{T} \sum_{t=1}^T Z_t \right| + \frac{1}{T} \sum_{t=1}^{T-1} |R(\theta_{t+1}, f_t) - R(\theta_t, f_t)|. \quad (*)$$

Step 3: Bounding one-step risk variation by drift. Fix t and condition on \mathcal{F}_{t-1} , so that (θ_t, f_t) is deterministic. Lemma 11 applied with $\theta' = \theta_{t+1}$ and $\theta = \theta_t$ gives, for each realization,

$$|R(\theta_{t+1}, f_t) - R(\theta_t, f_t)| \leq L_p d_F(\theta_{t+1}, \theta_t).$$

Taking conditional expectations and using the one-step Fisher bound

$$\mathbb{E}[d_F(\theta_{t+1}, \theta_t) \mid \mathcal{F}_{t-1}] \leq d_t + \alpha \kappa_t^{(\mathcal{M})}, \quad (19)$$

we obtain

$$\mathbb{E}[|R(\theta_{t+1}, f_t) - R(\theta_t, f_t)| \mid \mathcal{F}_{t-1}] \leq C_1 d_t + C_2 \kappa_t^{(\mathcal{M})},$$

for suitable constants $C_1, C_2 > 0$ depending only on $(L_p, \Theta, g_\theta, \alpha)$. Dropping the conditioning yields

$$\mathbb{E}|R(\theta_{t+1}, f_t) - R(\theta_t, f_t)| \leq C_1 d_t + C_2 \kappa_t^{(\mathcal{M})}. \quad (**)$$

Step 4: Combine sampling and drift terms. Taking expectations in $(*)$ and applying the bounds from Steps 1 and 3 gives

$$\begin{aligned} \mathbb{E}|\hat{R}_T - R_T| &\leq \mathbb{E} \left| \frac{1}{T} \sum_{t=1}^T Z_t \right| + \frac{1}{T} \sum_{t=1}^{T-1} \mathbb{E}|R(\theta_{t+1}, f_t) - R(\theta_t, f_t)| \\ &\leq C_0 T^{-1/2} + \frac{C_1}{T} \sum_{t=1}^{T-1} d_t + \frac{C_2}{T} \sum_{t=1}^{T-1} \kappa_t^{(\mathcal{M})}. \end{aligned}$$

Since the constants (C_0, C_1, C_2) do not depend on the choice of learner (f, π) , the same bound holds uniformly over all drift–feedback processes in the model class. This is exactly the claim of Theorem 13. (The dependence on T is only through the scaling.) ■

A.4 Proof of Theorem 15 (Lower Bound)

Proof

Step 1: Local model and geodesic. As in previous arguments, it suffices to work in a one-dimensional exponential family

$$p_\theta(x) = \exp(\theta x - A(\theta)) h(x), \quad \theta \in \Theta \subset \mathbb{R},$$

with $A''(\theta) = I(\theta)$ bounded above and below on the compact interval Θ . Thus $g_\theta = I(\theta)$ has bounded curvature and satisfies Assumption 1.

Because the model is one-dimensional, we may reparameterize Θ in *Fisher arclength coordinates* around θ_0 . In this coordinate, the Fisher metric at θ_0 is one, and the unit-speed geodesic through θ_0 has the simple form

$$\gamma(s) = \theta_0 + s, \quad s \in [-1, 1].$$

We take the environment dynamics in this arclength coordinate to be

$$\theta_{t+1} = F(\theta_t, u_t) = \theta_t + u_t,$$

with no exogenous noise. Hence $d_t \equiv 0$, and the endogenous drift magnitude satisfies

$$\kappa_t^{(\mathcal{M})} = \|u_t\|_{g_{\theta_t}} = |u_t|,$$

since in one dimension the Fisher metric in arclength coordinates is identically 1.

Step 2: Block structure and codebook. Fix a small step size $\delta > 0$ (to be specified later) and let m be the number of two-step blocks. Assume $2m \leq T$ and partition $\{1, \dots, 2m\}$ into blocks

$$B_j = \{2j-1, 2j\}, \quad j = 1, \dots, m,$$

keeping $\theta_t = \theta_0$ and $u_t = 0$ for $t > 2m$.

Let $V \subset \{-1, +1\}^m$ be a binary code of length m and minimum Hamming distance at least βm , with $|V| \geq 2^{\alpha m}$ for some $\alpha, \beta > 0$ (via the Gilbert–Varshamov bound, MacWilliams and Sloane, 1977). Each $v = (v_1, \dots, v_m) \in V$ indexes a distinct drift–feedback process.

Step 3: Feedback policies and drift trajectories. For each codeword $v \in V$, define a *deterministic open-loop feedback policy*

$$\pi_t^{(v)}(\mathcal{F}_t) := u_t^{(v)},$$

i.e. the policy outputs the prescribed control regardless of the filtration. This is a valid policy in the endogenous-drift model, as it is measurable with respect to \mathcal{F}_t .

Within block j define the controls

$$u_{2j-1}^{(v)} = v_j \delta, \quad u_{2j}^{(v)} = -v_j \delta, \quad u_t^{(v)} = 0 \text{ for } t > 2m.$$

Initialize $\theta_1 = \theta_0$ and evolve according to $\theta_{t+1} = \theta_t + u_t$. A simple induction then yields

$$\theta_{2j-1}^{(v)} = \gamma(0) = \theta_0, \quad \theta_{2j}^{(v)} = \gamma(v_j \delta),$$

while $\theta_t^{(v)} = \theta_0$ for $t > 2m$. Thus each block performs a Fisher geodesic loop of length 2δ , and the total endogenous drift satisfies

$$\sum_{t=1}^T \kappa_t^{(\mathcal{M})}(v) = \sum_{j=1}^m (|u_{2j-1}^{(v)}| + |u_{2j}^{(v)}|) = 2m\delta.$$

Given a budget $C > 0$, choose m so that $2m\delta \leq C$. This ensures $C_T(P_v) \leq C$ for each process in the family.

Step 4: Separation in trajectory-averaged risk. Let $\mathcal{L}_t(\theta)$ denote the population loss at time t . Define the trajectory-averaged risk

$$R_T(P_v) = \frac{1}{T} \sum_{t=1}^T \mathcal{L}_t(\theta_t^{(v)}).$$

Smoothness of the loss in regular exponential families yields the first-order expansion

$$\mathcal{L}_t(\gamma(\delta)) - \mathcal{L}_t(\gamma(-\delta)) = 2\delta \mathcal{L}'_t(\theta_0) + O(\delta^2).$$

Choose a model/loss pair with $|\mathcal{L}'_t(\theta_0)| \geq c_0 > 0$. Then whenever $v_j \neq w_j$,

$$|\mathcal{L}_{2j}(\theta_{2j}^{(v)}) - \mathcal{L}_{2j}(\theta_{2j}^{(w)})| \geq c_\ell \delta$$

for some $c_\ell > 0$ and all sufficiently small δ . Since distinct codewords differ in at least βm blocks,

$$|R_T(P_v) - R_T(P_w)| \geq \frac{\beta m c_\ell \delta}{T} \asymp \frac{m\delta}{T} \asymp \frac{C_T}{T}.$$

Step 5: KL divergence. Because samples are conditionally independent given the trajectory,

$$D_{\text{KL}}(P_v \| P_w) = \sum_{t=1}^T D_{\text{KL}}(p_{\theta_t^{(v)}} \| p_{\theta_t^{(w)}}).$$

Trajectories agree at all odd times and for all $t > 2m$. Thus only even indices $t = 2j$ in disagreeing blocks contribute. In exponential families,

$$D_{\text{KL}}(p_{\theta+\delta} \| p_{\theta-\delta}) = \frac{1}{2} I(\tilde{\theta})(2\delta)^2 \leq C_I \delta^2,$$

with $\tilde{\theta}$ between $\theta \pm \delta$. Hence for $v \neq w$,

$$D_{\text{KL}}(P_v \| P_w) \leq C_I (\# \text{ disagreeing blocks}) \cdot \delta^2 \leq C_I m \delta^2.$$

Since $|V| \geq 2^{\alpha m}$ we have $\log |V| \geq \alpha m \log 2$. Choosing δ sufficiently small ensures

$$D_{\text{KL}}(P_v \| P_w) \leq \frac{\alpha}{4} \log |V|,$$

i.e. the Fano separation condition.

Step 6: Fano inequality. Let \hat{R}_T be any estimator. A standard multi-hypothesis Fano inequality (for example Yu, 1997) yields

$$\inf_{\hat{R}_T} \sup_{v \in V} \mathbb{E}_{P_v} \left[\left| \hat{R}_T - R_T(P_v) \right| \right] \geq c \inf_{v \neq w} |R_T(P_v) - R_T(P_w)| \geq c' \frac{C_T}{T},$$

for constants $c, c' > 0$ depending only on $(L_p, \sigma, \Theta, g_\theta)$. Since each P_v satisfies $C_T \leq C$, the same lower bound holds for the full minimax problem over all drift-feedback processes with budget C .

Finally, restricting to processes with $C_T \equiv 0$ recovers the classical i.i.d. lower bound of order $T^{-1/2}$. Combining the two regimes yields the claimed minimax rate $\max(T^{-1/2}, \frac{C}{T})$. \blacksquare

Proof of Corollary 16 (Reproducibility Speed Limit)

Proof Let $C_T = \sum_{t=1}^T (d_t + \alpha \kappa_t^{(\mathcal{M})})$ denote the cumulative reproducibility budget, and suppose $C_T \leq C$ for some constant $C > 0$.

Step 1: Upper bound. From Theorem 13, for any learner (f, π) the empirical risk estimator defined above satisfies

$$\mathbb{E} |\hat{R}_T(f, \pi) - R_T(f, \pi)| \leq \frac{C_0}{\sqrt{T}} + \frac{C_1}{T} \sum_{t=1}^{T-1} d_t + \frac{C_2}{T} \sum_{t=1}^{T-1} \kappa_t^{(\mathcal{M})}.$$

Since $d_t, \kappa_t^{(\mathcal{M})} \geq 0$ and $\sum_t (d_t + \alpha \kappa_t^{(\mathcal{M})}) \leq C$, we have $\sum_t d_t + \sum_t \kappa_t^{(\mathcal{M})} \leq C'$ for $C' = (1 + 1/\alpha)C$. Absorbing constants gives the uniform upper bound

$$\mathbb{E} |\hat{R}_T - R_T| \leq C_u \left(T^{-1/2} + \frac{C}{T} \right), \quad (\text{A.20})$$

with C_u depending only on $(L_p, L_{\max}, \Theta, g_\theta, \alpha)$.

Step 2: Lower bound. Theorem 15 constructs a family of processes satisfying Assumption 1 for which

$$\inf_{\hat{R}_T(f, \pi)} \sup \mathbb{E} |\hat{R}_T - R_T(f, \pi)| \geq c_1 \frac{1}{T} \sum_{t=1}^{T-1} \kappa_t^{(\mathcal{M})} - c_2 T^{-1/2}.$$

Since $\sum_t \kappa_t^{(\mathcal{M})} \leq C/\alpha$ for $C_T \leq C$, this gives

$$\inf_{\hat{R}_T(f, \pi): C_T \leq C} \sup \mathbb{E} |\hat{R}_T - R_T(f, \pi)| \geq C_\ell \left(\frac{C}{T} + T^{-1/2} \right), \quad (\text{A.21})$$

for constants $C_\ell > 0$ depending on $(L_p, L_{\max}, \Theta, g_\theta)$.

Step 3: Combine upper and lower bounds. Together, inequalities (A.20) and (A.21) imply that for all sufficiently large T ,

$$\inf_{\hat{R}_T(f, \pi): C_T \leq C} \sup \mathbb{E} |\hat{R}_T - R_T(f, \pi)| = \Theta \left(T^{-1/2} + \frac{C}{T} \right),$$

with constants depending only on the problem parameters listed above. ■

Proofs of Limiting Regimes (Stationary and Classical Limits)

Lemma 17 (i.i.d. regime) *If $d_t \equiv 0$ and $J_u F \equiv 0$ for all t , then the sequence $\{\theta_t\}$ is constant, $p_{\theta_t} = p_{\theta_0}$, and the samples (x_t, y_t) are i.i.d. from p_{θ_0} . In this case,*

$$\mathbb{E} |\hat{R}_T - R_T| = \mathbb{E} \left| \frac{1}{T} \sum_{t=1}^T Z_t \right| \leq \frac{C_0}{\sqrt{T}},$$

by Corollary 6.

Proof Since $\theta_{t+1} = F(\theta_t, 0, 0) = \theta_t$, the distribution remains fixed, and the martingale differences Z_t in Theorem 13 are identically distributed and independent. Boundedness of ℓ gives the usual Hoeffding bound $O(T^{-1/2})$; nothing new happens here. ■

Lemma 18 (Exogenous–drift regime) *If $J_u F \equiv 0$ but $d_t > 0$, then the environment evolves independently of the learner. Theorem 13 reduces to*

$$\mathbb{E} |\hat{R}_T - R_T| \leq \frac{C_0}{\sqrt{T}} + \frac{C_1}{T} \sum_{t=1}^{T-1} d_t,$$

matching the classical variation–budget penalty of Besbes et al. (2015).

Proof With $J_u F = 0$, the endogenous term $\kappa_t^{(\mathcal{M})}$ vanishes. Only exogenous motion $d_t = \|\bar{\Delta}\theta_t\|_{g_{\theta_t}}$ remains, and its cumulative effect scales as $\sum_t d_t/T$, as shown in Theorem 13. ■

Lemma 19 (Performative equilibrium) *If both $d_t \equiv 0$ and $\kappa_t^{(\mathcal{M})} \equiv 0$, then the process is stationary and $\theta_t = \theta_0$ for all t . The generalization bound collapses to*

$$\mathbb{E} |\hat{R}_T - R_T| \leq \frac{C_0}{\sqrt{T}},$$

recovering the standard generalization rate under stationary sampling (Vapnik, 1998; Perdomo et al., 2020).

Proof This is immediate from Theorem 13 by substituting $d_t = \kappa_t^{(\mathcal{M})} = 0$. ■

Lemma 20 (Adaptive–data regime) *If $d_t \equiv 0$ but $\kappa_t^{(\mathcal{M})} > 0$, then all drift is policy–induced. Theorem 13 becomes*

$$\mathbb{E} |\hat{R}_T - R_T| \leq \frac{C_0}{\sqrt{T}} + \frac{C_2}{T} \sum_{t=1}^{T-1} \kappa_t^{(\mathcal{M})},$$

which parallels the adaptivity penalties in adaptive–data–analysis bounds (Dwork et al., 2015).

Proof With $d_t = 0$, only endogenous drift contributes to nonstationarity. Each step’s deviation $\mathbb{E}_{p_{\theta_t}} \ell(f_t) - \mathbb{E}_{p_{\theta_{t-1}}} \ell(f_{t-1})$ is controlled by Lemma 11 through the Fisher displacement $d_F(\theta_t, \theta_{t-1})$, which reduces here to $\alpha \kappa_t^{(\mathcal{M})}$. Summing over t yields the stated bound. ■

Synthesis. Lemmas 17–20 confirm that Theorem 13 specializes to the familiar regimes under their corresponding assumptions, reducing to

$$\mathbb{E} |\hat{R}_T - R_T| = O\left(T^{-1/2} + \frac{C_T}{T}\right),$$

where $C_T = \sum_t (d_t + \alpha \kappa_t^{(\mathcal{M})})$ encodes total distributional motion. In other words, nothing essential is lost when we summarize the behavior in terms of the reproducibility budget C_T .

Appendix B. Experiments

All experiments were implemented in Python 3.11 using NumPy, SciPy, and PyTorch (for the non-linear learner). Per-run integer seeds ensure deterministic reproduction of all reported results. Full source code, configuration files, and figure-generation scripts are available in the public repository (Section C).

Across all settings we record the environment trajectory $\{\theta_t\}$, the learner trajectory $\{f_t\}$, the empirical trajectory loss

$$\hat{R}_T = \frac{1}{T} \sum_{t=1}^T \ell(f_t(x_t), y_t),$$

and an approximation of the corresponding population loss $R_T = \frac{1}{T} \sum_{t=1}^T R(\theta_t, f_t)$, computed either in closed form (linear–Gaussian environment) or using clean mini-batches drawn from the latent generative model (nonlinear environment). The reported metric is the trajectory generalization gap $|\hat{R}_T - R_T|$. Across all experiments the learner’s training loss decreases substantially over time, ensuring the effects studied arise from drift rather than optimization instability.

B.1 Experiment 1: Stationary Rate and Drift Sensitivity

Objective. To verify that (i) in the absence of drift the trajectory generalization gap scales as $O(T^{-1/2})$, and (ii) under controlled exogenous or policy-sensitive drift, the gap increases proportionally to the accumulated drift magnitudes.

Setup. We simulate a linear–Gaussian environment $\theta_{t+1} = A\theta_t + Bu_t + \eta_t$, with $x_t \sim \mathcal{N}(\theta_t, \Sigma)$ and constant Fisher metric $g_\theta = \Sigma^{-1}$. Because the dynamics are linear, the drift increments decompose exactly into

$$d_t = \|\Delta\theta_t^{\text{exo}}\|_{g_\theta}, \quad \kappa_t^{(\mathcal{M})} = \|\Delta\theta_t^{\text{endo}}\|_{g_\theta}.$$

Population risk is available in closed form via $\text{tr}(\Sigma) + \|\theta_t - \hat{\mu}_t\|_2^2$.

Findings. The $\gamma = 0$ (i.i.d.) regime recovers the predicted $T^{-1/2}$ scaling. When exogenous or policy-sensitive drift is introduced, generalization gaps increase proportionally to the normalized drift magnitudes $T^{-1} \sum_t d_t$ and $T^{-1} \sum_t \kappa_t^{(\mathcal{M})}$.

B.2 Experiment 2: Additivity and Budget Collapse

Objective. To test the additive structure of drift contributions and the one-dimensional budget collapse predicted by Corollary 16.

Setup. Using the same linear–Gaussian simulator, we sweep a grid of exogenous drift amplitudes and feedback gains. For each run we record

$$\bar{d} = \frac{1}{T} \sum_{t=1}^T d_t, \quad \bar{\kappa} = \frac{1}{T} \sum_{t=1}^T \kappa_t^{(\mathcal{M})},$$

and fit the regression model

$$|\hat{R}_T - R_T| = b_0 + b_s T^{-1/2} + b_1 \bar{d} + b_2 \bar{\kappa}.$$

The ratio $\alpha_\star = b_2/b_1$ defines an empirical combined budget $C_T = \sum_t (d_t + \alpha_\star \kappa_t^{(\mathcal{M})})$.

Findings. A reduced model using only C_T/T matches the full three-term model with minimal loss, confirming the predicted budget collapse.

B.3 Experiment 3: Metric Alignment

Objective. To isolate the geometric role of optimization metric alignment.

Setup. We compare Euclidean and natural-gradient updates that achieve the same multiplicative decrease in a Euclidean quadratic objective $J(\theta) = \frac{1}{2}\|\theta\|_2^2$, under a fixed Fisher metric $g_\theta = \Sigma^{-1}$. Differences in cumulative Fisher path length

$$A = \sum_t \|\Delta\theta_t\|_{g_{\theta_t}}$$

reflect only the geometry of the update directions.

Findings. Natural-gradient trajectories incur substantially shorter Fisher path lengths than Euclidean ones, consistent with interpreting C_T as a measure of geometric motion.

B.4 Experiment 4: Nonlinear Speed–Limit Validation

Objective. To test whether the speed–limit relation persists in a nonlinear learner that violates the simplifying assumptions of the theory.

Latent environment and learner. Inputs are drawn as $x_t \sim \mathcal{N}(0, I_d)$ and labels as

$$y_t = \phi(x_t)^\top \theta_t + \sigma \xi_t, \quad \xi_t \sim \mathcal{N}(0, 1),$$

with ϕ a fixed random feature map. A two-layer MLP is trained using single-sample SGD. Population risk is approximated periodically using clean batches drawn from the latent generative model.

Drift construction. At each step an exogenous direction (unit length in the Fisher metric $G(\theta_t)$ of the latent model) and a policy-sensitive direction (derived from network disagreement on a probe batch) are proposed. Their expected Fisher lengths per step are C_{exo}/T and γ/T ; budget managers truncate increments to enforce these rates. We record surrogate drift magnitudes

$$d_t = \|\Delta\theta_t^{\text{exo}}\|_{G(\theta_t)}, \quad \kappa_t^{(\mathcal{M})} = \|\Delta\theta_t^{\text{endo}}\|_{G(\theta_t)}.$$

Calibration and validation. Calibration experiments fit

$$|\hat{R}_T - R_T| = b_0 + b_s T^{-1/2} + b_1 \bar{d} + b_2 \bar{\kappa},$$

yielding $\alpha_\star = b_2/b_1$. Held-out runs at larger horizons test the reduced model

$$|\hat{R}_T - R_T| = c_0 + c_1 T^{-1/2} + c_2 (C_T/T).$$

The reduced model accurately predicts the empirical gaps despite the nonlinear learner dynamics.

Appendix C. Reproducibility Artifacts

A complete repository containing source code, configuration files, and figure-generation scripts is available at:

<https://github.com/fiazaich/Learning-under-Drift>

References

- P.-A. Absil, R. Mahony, and R. Sepulchre. *Optimization Algorithms on Matrix Manifolds*. Princeton University Press, Princeton, NJ, USA, 2008. ISBN 978-0-691-13298-3.
- Pierre Alquier and Benjamin Guedj. Simpson’s paradox and the dependent pac-bayes bound. *Entropy*, 20(6):466, 2018. doi: 10.3390/e20060466.

- Shun-ichi Amari. Natural gradient works efficiently in learning. *Neural Computation*, 10(2):251–276, 1998. doi: 10.1162/089976698300017746.
- Shun-ichi Amari. *Information Geometry and Its Applications*. Springer, 2016. doi: 10.1007/978-4-431-55978-8.
- Shun-ichi Amari and Hiroshi Nagaoka. *Methods of Information Geometry*, volume 191 of *Translations of Mathematical Monographs*. American Mathematical Society & Oxford University Press, 2000. ISBN 978-0-8218-4302-4.
- Karl Johan Åström and Richard M. Murray. *Feedback Systems: An Introduction for Scientists and Engineers*. Princeton University Press, Princeton, NJ, 2008. ISBN 978-0-691-13576-2.
- Raef Bassily, Kobbi Nissim, Adam Smith, Thomas Steinke, Uri Stemmer, and Jonathan Ullman. Algorithmic stability for adaptive data analysis? In Yishay Mansour and Daniel Wichs, editors, *Proceedings of the 48th Annual ACM SIGACT Symposium on Theory of Computing (STOC 2016)*, pages 1046–1059, Cambridge, MA, USA, 2016. Association for Computing Machinery. doi: 10.1145/2897518.2897566. URL <https://doi.org/10.1145/2897518.2897566>.
- Bernard Bercu, Bernard Delyon, and Emmanuel Rio. *Concentration Inequalities for Sums and Martingales*. SpringerBriefs in Mathematics. Springer International Publishing, 2015. ISBN 978-3319220987. doi: 10.1007/978-3-319-22099-4.
- Omar Besbes, Yonatan Gur, and Assaf Zeevi. Non-stationary stochastic optimization. *Operations Research*, 63(5):1227–1244, 2015. doi: 10.1287/opre.2015.1408.
- Gilles Blanchard, Aniket Anand Deshmukh, Urun Doğan, Gyemin Lee, and Clayton Scott. Domain generalization by marginal transfer learning. *Journal of Machine Learning Research*, 22(17-679): 1–55, 2021. URL <https://jmlr.org/papers/volume22/17-679/17-679.pdf>.
- Stéphane Boucheron, Gábor Lugosi, and Pascal Massart. *Concentration Inequalities: A Nonasymptotic Theory of Independence*. Oxford University Press, Oxford, 2013. doi: 10.1093/acprof:oso/9780199535255.001.0001.
- Cynthia Dwork, Vitaly Feldman, Moritz Hardt, Toniann Pitassi, Omer Reingold, and Aaron Roth. Preserving statistical validity in adaptive data analysis. In *Advances in Neural Information Processing Systems*, volume 28, 2015. URL https://proceedings.neurips.cc/paper_files/paper/2015/file/bad5f33780c42f2588878a9d07405083-Paper.pdf.
- Eyal Even-Dar and Yishay Mansour. Learning rates for q-learning. *Journal of Machine Learning Research*, 5(Dec):1–25, 2003. URL <https://www.jmlr.org/papers/v5/evendar03a.html>.
- Sebastian Goldt and Udo Seifert. Stochastic thermodynamics of learning. *Physical Review Letters*, 118(1):010601, 2017. doi: 10.1103/PhysRevLett.118.010601. URL <https://doi.org/10.1103/PhysRevLett.118.010601>.
- Zachary Izzo, Lexing Ying, and James Zou. How to learn when data reacts to your model: Performative gradient descent. In Marina Meila and Tong Zhang, editors, *Proceedings of the 38th International Conference on Machine Learning*, volume 139 of *Proceedings of Machine Learning Research*, pages 4641–4650. PMLR, 2021. URL <https://proceedings.mlr.press/v139/izzo21a.html>.
- Meena Jagadeesan, Tijana Zrnic, and Celestine Mendler-Dünner. Regret minimization with performative feedback. In Kamalika Chaudhuri, Stefanie Jegelka, Le Song, Csaba Szepesvari, Gang Niu, and Sivan Sabato, editors, *Proceedings of the 39th International Conference on Machine Learning*, volume 162 of *Proceedings of Machine Learning Research*, pages 9760–9785. PMLR, Jul 17–23 2022. URL <https://proceedings.mlr.press/v162/jagadeesan22a.html>.

- Vitaly Kuznetsov and Mehryar Mohri. Time series prediction and online learning. In Vitaly Feldman, Alexander Rakhlin, and Ohad Shamir, editors, *29th Annual Conference on Learning Theory*, volume 49 of *Proceedings of Machine Learning Research*, pages 1190–1213, Columbia University, New York, NY, USA, 23–26 Jun 2016. PMLR.
- John M. Lee. *Riemannian Manifolds: An Introduction to Curvature*, volume 176 of *Graduate Texts in Mathematics*. Springer-Verlag, New York, 1997. ISBN 0-387-98271-X, 978-0-387-98271-7. doi: 10.1007/b98852.
- Jiachun Li, David Simchi-Levi, and Yunxiao Zhao. Optimal adaptive experimental design for estimating treatment effect, 2024. URL <https://arxiv.org/abs/2410.05552>.
- F. J. MacWilliams and N. J. A. Sloane. *The Theory of Error-Correcting Codes*. North-Holland, Amsterdam, 1977. ISBN 978-0444851932.
- James Martens. New insights and perspectives on the natural gradient method. *Journal of Machine Learning Research*, 21:1–76, 2020. URL <https://www.jmlr.org/papers/v21/17-678.html>. JMLR Paper No. 17-678.
- Mehryar Mohri and Andrés Muñoz Medina. New analysis and algorithm for learning with drifting distributions. In Nader H. Bshouty, Gilles Stoltz, Nicolas Vayatis, and Thomas Zeugmann, editors, *Algorithmic Learning Theory (ALT 2012)*, volume 7568 of *Lecture Notes in Computer Science*, pages 124–138. Springer, Berlin, Heidelberg, 2012. ISBN 978-3-642-34105-2, 978-3-642-34106-9. doi: 10.1007/978-3-642-34106-9_13.
- Pedro A. Ortega and Daniel A. Braun. Thermodynamics as a theory of decision-making with information-processing costs. *Proceedings of the Royal Society A: Mathematical, Physical and Engineering Sciences*, 469(2153), 2013. doi: 10.1098/rspa.2012.0683.
- German I. Parisi, Ronald Kemker, Jose L. Part, Christopher Kanan, and Stefan Wermter. Continual lifelong learning with neural networks: A review. *Neural Networks*, 113:54–71, 2019. doi: 10.1016/j.neunet.2019.01.012. URL <https://doi.org/10.1016/j.neunet.2019.01.012>.
- Juan C. Perdomo, Tijana Zrnic, Celestine Mendler-Dünner, and Moritz Hardt. Performative prediction. In *Proceedings of the 37th International Conference on Machine Learning (ICML)*, pages 7599–7609. PMLR, 2020. URL <https://proceedings.mlr.press/v119/perdomo20a.html>.
- C. R. Rao. Information and the accuracy attainable in the estimation of statistical parameters. *Bulletin of the Calcutta Mathematical Society*, 37:81–91, 1945.
- Pascanu Razvan, Mikolov Tomas, and Bengio Yoshua. On the difficulty of training recurrent neural networks. In Dasgupta Sanjoy and McAllester David editors, *Proceedings of the 30th International Conference on Machine Learning*, volume 28 of *Proceedings of Machine Learning Research*, pages 1310–1318, Atlanta, Georgia, USA, 2013. PMLR.
- Ryan Rogers, Aaron Roth, Adam Smith, Nathan Srebro, Om Thakkar, and Blake Woodworth. Guaranteed validity for empirical approaches to adaptive data analysis. In Silvia Chiappa and Roberto Calandra, editors, *Proceedings of the Twenty Third International Conference on Artificial Intelligence and Statistics*, volume 108 of *Proceedings of Machine Learning Research*, pages 2830–2840. PMLR, Aug 26–28 2020. URL <https://proceedings.mlr.press/v108/rogers20a.html>.
- Daniel Russo and James Zou. Controlling bias in adaptive data analysis using information theory. In Arthur Gretton and Christian C. Robert, editors, *Proceedings of the 19th International Conference on Artificial Intelligence and Statistics*, volume 51 of *Proceedings of Machine Learning Research*, pages 1232–1240, Cadiz, Spain, 09–11 May 2016. PMLR. URL <https://proceedings.mlr.press/v51/russo16.html>.

- Yevgeny Seldin, Nicolò Cesa-Bianchi, Peter Auer, and John Shawe-Taylor. Pac-bayesian inequalities for martingales. *IEEE Transactions on Information Theory*, 58(12):7086–7093, 2012. doi: 10.1109/TIT.2012.2212437.
- Shai Shalev-Shwartz and Shai Ben-David. *Understanding Machine Learning: From Theory to Algorithms*. Cambridge University Press, USA, 2014. ISBN 1107057132.
- Susanne Still, David A Sivak, Gavin Bell, and Gavin E Crooks. Thermodynamics of prediction. *Physical Review Letters*, 109(12):120604, 2012. doi: 10.1103/PhysRevLett.109.120604. URL <https://link.aps.org/doi/10.1103/PhysRevLett.109.120604>.
- Richard S. Sutton and Andrew G. Barto. *Reinforcement Learning: An Introduction*. The MIT Press, second edition, 2018. URL <http://incompleteideas.net/book/the-book-2nd.html>.
- Vladimir N. Vapnik. *Statistical Learning Theory*. Wiley, New York, 1998. ISBN 978-0-471-03003-4.
- Aolin Xu and Maxim Raginsky. Information-theoretic analysis of generalization capability of learning algorithms. NIPS’17, page 2521–2530, Red Hook, NY, USA, 2017. Curran Associates Inc. ISBN 9781510860964.
- B. Yu. Assouad, fano, and le cam. In *Festschrift for Lucien Le Cam*, pages 423–435. Springer, 1997.
- Peng Zhao, Yu-Jie Zhang, Lijun Zhang, and Zhi-Hua Zhou. Adaptivity and non-stationarity: Problem-dependent dynamic regret for online convex optimization. *Journal of Machine Learning Research*, 25(98):1–52, 2024. URL <https://www.jmlr.org/papers/v25/21-0748.html>.
- N. N. Čencov. *Statistical Decision Rules and Optimal Inference*, volume 53 of *Translations of Mathematical Monographs*. American Mathematical Society, Providence, RI, 1982. ISBN 978-0-8218-4502-8.